*Materials* **2012**, *5*, 1125-1154; doi:10.3390/ma5061125

OPEN ACCESS

*materials*

**ISSN 1996-1944**

www.mdpi.com/journal/materials

*Review*

# Two Decades of Negative Thermal Expansion Research: Where Do We Stand?

**Cora Lind**

Department of Chemistry, the University of Toledo, Toledo, OH 43606, USA;
E-Mail: cora.lind@utoledo.edu; Tel.: +1-419-530-1505; Fax: +1-419-530-4033

*Received: 16 April 2012; in revised form: 1 June 2012 / Accepted: 15 June 2012 / Published: 20 June 2012*

**Abstract:** Negative thermal expansion (NTE) materials have become a rapidly growing area of research over the past two decades. The initial discovery of materials displaying NTE over a large temperature range, combined with elucidation of the mechanism behind this unusual property, was followed by predictions that these materials will find use in various applications through controlled thermal expansion composites. While some patents have been filed and devices built, a number of obstacles have prevented the widespread implementation of NTE materials to date. This paper reviews NTE materials that contract due to transverse atomic vibrations, their potential for use in controlled thermal expansion composites, and known problems that could interfere with such applications.

**Keywords:** negative thermal expansion; mechanisms; composites; challenges

## 1. Introduction

Over the past two decades, the field of negative thermal expansion (NTE) has rapidly expanded [1–24]. This is evident when tracking the number of publications on "negative thermal expansion" over the past 50 years (Figure 1), and the fact that special issues of journals have been devoted to the topic [25]. Such sudden growth of new research fields is often related to the discovery of a new phenomenon or a new class of compounds. However, the first observation of compounds that contract upon heating dates back several hundred years to the discovery of the "density anomaly of water". Shrinkage of a solid was first documented by Scheel in 1907 for quartz and vitreous silica at low temperatures [26,27], and additional reports of materials that contract over various temperature ranges appeared in the literature throughout the years. This included research on lithium aluminum silicates

(LAS) in the 1950s [28,29], and the discovery of the sodium zirconate phosphate (NZP) family in the 1980s [30–33]. These materials can show either positive or negative volume expansion depending on composition, as contraction is observed along only one or two of the crystallographic axes. They were usually referred to as "low expansion ceramics" instead of "NTE materials", and the term "NTE" was used only sporadically between the 1960s and the 1990s. Notably, the expansion behavior of $ZrW_2O_8$ [34], which has since become one of the most researched NTE compounds and is often used as the key representative of NTE, was measured over the temperature range 323 to 973 K in 1968 [35]. However, this behavior remained a peculiarity until the mid 1990's, when Sleight's group could show that the NTE behavior of several families of compounds was intimately related to their crystal structures [1–3,5]. This included the first observation of inherently isotropic NTE over a large temperature range in cubic $ZrV_2O_7$ [1] and $ZrW_2O_8$ [3]. Theoretical and experimental studies soon established sophisticated models that can be used to explain this unusual behavior for a number of framework compounds [6,8,11,12,15,16,21,36–44]. This opened up the targeted synthesis of new NTE compositions, and established NTE as a specialized field of research. Several new families of materials in which NTE is caused by different mechanisms have been discovered as well, but they are outside the scope of this review. Compounds belonging to the LAS and NZP families will not be discussed in detail either, as they were already well established as low expansion ceramics by the time NTE became a separate field of research.

**Figure 1.** Number of publications per year based on a Web of Science search for "negative thermal expansion". Note that early publications related to the field are missing as they did not use NTE as a keyword.

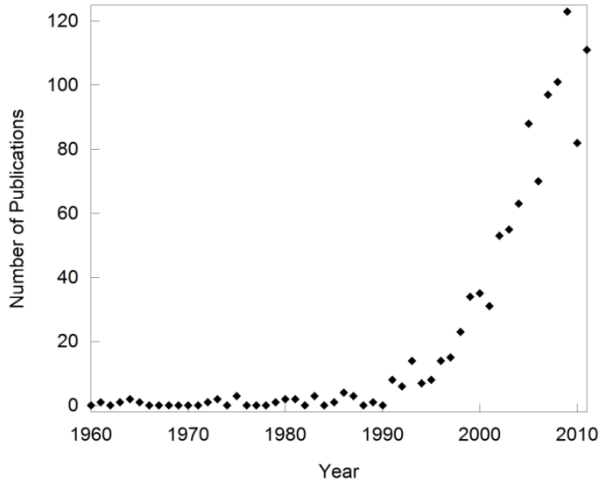


The potential uses of NTE materials in controlled thermal expansion composites were readily recognized, and possible applications ranging from fiber optics coatings, electronics and mirror substrates to tooth fillings were proposed [9,45–48]. However, some limitations of different NTE materials became quickly apparent, one of which relates to the fact that many NTE compounds contain transition metals, which would increase product cost. In addition, problems with stability under processing and use conditions, and incompatibilities with other composite components were encountered [49–52]. These challenges have become active areas of research, and efforts are directed

at the discovery of new NTE materials, improvements of properties of existing materials, modification of particles to achieve compatibility, and establishing processing conditions for formation of homogeneous composites.

## 2. Negative Thermal Expansion Due to Transverse Vibrations

The expansion behavior of most NTE materials that were known or discovered in the 1990's can be explained based on their crystal structure. These compounds are composed of rigid $MO_4$ tetrahedra and/or $MO_6$ octahedra, which are connected by corner-sharing oxygen atoms. Due to the corner-sharing nature of the frameworks, the polyhedra can undergo concerted tilting or rocking motions when transverse vibrations of the corner-sharing oxygen atoms are excited. For approximately linear M-O-M linkages, this process leads to a reduction of second-nearest-neighbor distances, and can result in linear or volume NTE (Figure 2). This mechanism operates in materials belonging to the zirconium tungstate family [3,53,54], scandium tungstate family [5,23], zirconium vanadate family [1], a number of zeolites and aluminum phosphates [24,55,56], Prussian blue analogs [57,58], and a few other materials [59]. Early theoretical models treated the polyhedra as rigid units, and referred to the concerted lattice vibrations as "rigid unit modes", or RUMs [37,59–62].

The RUM model can adequately describe the NTE behavior observed in $ZrW_2O_8$ and some zeolites, however, the polyhedra in the $ZrV_2O_7$ and $Sc_2W_3O_{12}$ families have been found to distort. These distortions have resulted in more varied values for expansion coefficients for the same structural family depending on the size and rigidity of the polyhedra. Similar behavior has also been observed in some cyanides, where the CN linkages undergo vibrations that lead to a shortening of metal-metal distances. Due to the greater flexibility of the two-atom linker, the expansion behavior can vary widely from strong NTE to positive expansion. In some cyanide frameworks, other mechanisms also contribute to NTE behavior.

**Figure 2.** Schematics of vibrational modes leading to NTE: (**a**) Transverse vibrational motion of an oxygen atom in a M-O-M linkage causing a decrease of the metal-metal distance; (**b**) cooperative rocking of polyhedra causing a decrease in average metal-metal distances.

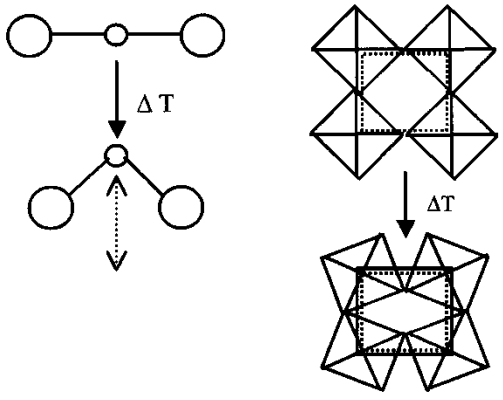


The transverse vibration mechanism can also be expressed in terms of low energy librational phonon modes with large, negative Grüneisen parameters ($\gamma$). The presence of such modes has been

proven experimentally through specific heat [8,39,63], phonon density of states [6,10,39], and total neutron scattering studies [12,64,65] Because the overall expansion behavior of a compound depends on the relative contributions from all phonons, not all materials with low energy phonon modes with negative $\gamma_i$ values will exhibit NTE behavior. A feature necessary for the occurrence of NTE is the presence of low energy phonons with negative $\gamma_i$ values, and a phonon gap that separates these modes from the high energy phonons also present in the structure [21].

### *2.1. $ZrW_2O_8$ Family*

While a number of materials have been found to contract upon heating, the compound zirconium tungstate has become almost synonymous with the expression NTE. $ZrW_2O_8$ was first discovered in 1959 by Graham [34] and its unusual expansion behavior was documented by Martinek and Hummel in 1968 [35] At that time, the strong contraction was regarded as equally detrimental as strong positive expansion, and the search for zero expansion materials moved on to different materials. In 1995, Auray solved the crystal structure of $ZrW_2O_8$ [66], and in 1996, Sleight's group showed that the structure is responsible for the strong NTE behavior observed from 0.3 to 1050 K [3]. The material is thermodynamically stable between 1378 and 1508 K, but can be quenched and remains metastable up to 1050 K. The structure is composed of corner-sharing $ZrO_6$ octahedra and $WO_4$ tetrahedra, with each $ZrO_6$ connected to six $WO_4$ units, while each tetrahedron is connected to only three octahedra, leaving one terminal oxygen. The $WO_4$ units are oriented along the body diagonal of the cubic cell, and can be described as $W_2O_8$ units with one 4-coordinated tungsten, and a tungsten with 4+1 coordination due to a long range contact with an oxygen from the neighboring tungsten (Figure 3a).

**Figure 3.** Crystal structures of (**a**) $\alpha$-$ZrW_2O_8$; (**b**) $ZrV_2O_7$ (ideal high temperature structure); bright: $ZrO_6$ octahedra; dark: $WO_4$/$VO_4$ tetrahedra. The structures only differ in the orientation and connectivity of the polyhedra.

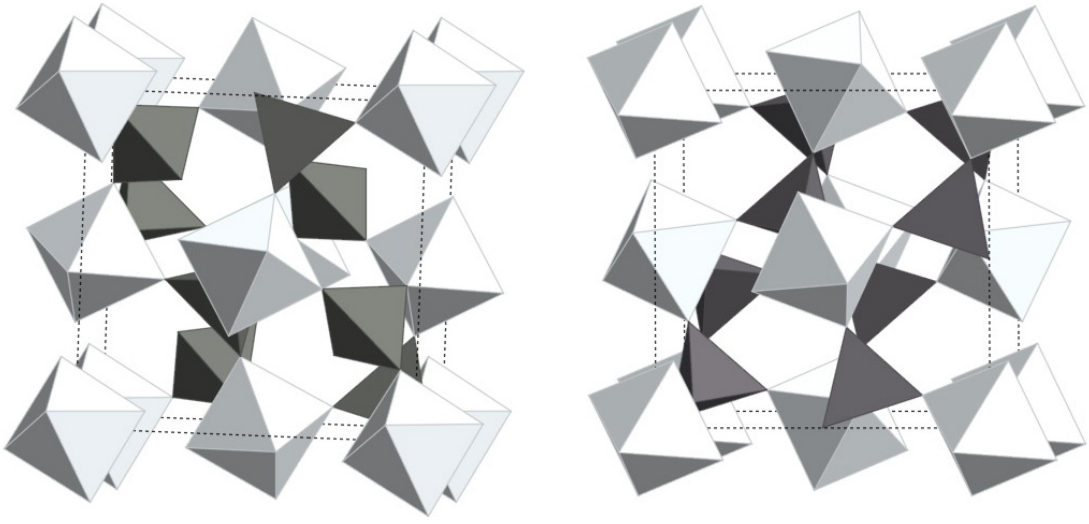

(**a**) (**b**)

The material's contraction is inherently isotropic due to its cubic structure, with $\alpha_l$ values of $-9.1 \times 10^{-6}$ $K^{-1}$ below 350 K, and $-5.0 \times 10^{-6}$ $K^{-1}$ above 450 K. The magnitude of expansion changes due to an order-disorder phase transition at 448 K ($\alpha$-$ZrW_2O_8$ to $\beta$-$ZrW_2O_8$), but the cubic symmetry is

preserved (space groups $P2_13$ and $Pa\bar{3}$, respectively). The transition involves a reorientation of the $WO_4$ tetrahedra, and causes a discontinuity in the otherwise linear expansion behavior. The $ZrW_2O_8$ structure supports rigid unit modes, which are responsible for the strong NTE over a large temperature range. Phonon density of states measurements revealed significant contributions from very low energy modes with negative Grüneisen parameters, and the presence of a gap between low and high energy phonons [6,8,39].

### 2.1.1. Substitution of $ZrW_2O_8$

Both metal sites in the $ZrW_2O_8$ family can be substituted. Shortly after the pivotal $ZrW_2O_8$ paper, NTE compounds prepared by substitution of Hf on the Zr site and Mo on the W site were reported [53,54,67]. The $HfW_2O_8$ analog shows essentially identical expansion behavior with respect to the magnitude of $\alpha$, and only a small increase in the temperature of the order-disorder phase transition ($T_{trs}$ = 463 K) is observed. In contrast, $ZrMo_2O_8$ and $HfMo_2O_8$ do not undergo a transition to the ordered $P2_13$ structure, but adopt space group $Pa\bar{3}$ at all temperatures. A transition from dynamic to static oxygen disorder occurs at low temperatures, which increases the magnitude of NTE ($\alpha_l \approx -8 \times 10^{-6}$ K$^{-1}$ below 200 K, and $-5 \times 10^{-6}$ K$^{-1}$ from 200 to 600 K) [68]. Early research suggested that both molybdates were metastable at all temperatures and could only be obtained by dehydration and topotactic recrystallization from a hydrated precursor ($AM_2O_7(OH)_2 \cdot 2(H_2O)$; A = Zr, Hf; M = Mo, W) [54,69,70]. However, recent *in situ* diffraction experiments provide evidence that cubic $ZrMo_2O_8$ may be stable in sealed tubes above 1350 K. The disappearance of diffraction peaks at higher temperatures was interpreted as melting, as little to no formation of $ZrO_2$ was observed at 1460 K, and the cubic phase recrystallized during quenching experiments [71]. The sealed environment is necessary to prevent evaporation of $MoO_3$, which becomes volatile above 1000 K under atmospheric pressure.

The complete range of $Zr_{1-x}Hf_xW_{2-y}Mo_yO_8$ solid solutions ($0 \le x \le 1$; $0 \le y \le 2$) can be synthesized either from $AM_2O_7(OH)_2 \cdot 2(H_2O)$ precursors or by solid-state methods [72,73]. This is not surprising, as $Zr^{4+}$ and $Hf^{4+}$ (0.72 Å and 0.71 Å in octahedral coordination) and $Mo^{6+}$ and $W^{6+}$ (0.55 Å and 0.56 Å in tetrahedral coordination) have very similar ionic radii to each other. Like for the pure tungstates, hafnium substitution does not significantly change the expansion and phase transition behavior of the solid solutions. In contrast, the molybdenum content strongly influences formation of the ordered $P2_13$ phase. For compositions with more than 50% tungsten, the order-disorder ($\alpha$ to $\beta$) transition is observed, and the temperature varies linearly with composition. $ZrMoWO_8$ remains in the $Pa\bar{3}$ structure when rapidly cooled, but formation of the $P2_13$ polymorph was observed at about 270 K upon slow cooling [74]. No ordered phase has been reported for $y > 1$, although it is possible that ordering was not detected for some compositions due to slow kinetics. While $ZrW_2O_8$ adopts a fully ordered structure at low temperatures, some local disordered regions remain even to the lowest temperatures for $ZrMoWO_8$.

Substitution of $ZrW_2O_8$ by elements other than Hf and Mo is also possible, although solubility is limited in all cases even when metals with identical charges are chosen. The highest substitution levels have been achieved with $Sn^{4+}$ in $Zr_{0.7}Sn_{0.3}W_2O_8$ [75]. The solubility of $Ti^{4+}$ is limited to about 5% due to its much smaller ionic radius (octahedrally coordinated $Ti^{4+}$: 0.61 Å), which induces lattice strain [76] In both cases, a reduction in the $\alpha$-$\beta$ phase transition temperature was observed (400 K for

$Zr_{0.7}Sn_{0.3}W_2O_8$ and 405 K for $Zr_{0.95}Ti_{0.05}W_2O_8$, respectively). The expansion coefficients show limited dependence on composition, and fall around $-10 \times 10^{-6}$ $K^{-1}$ for materials in the α-phase, and $-5 \times 10^{-6}$ $K^{-1}$ for materials in the β-phase.

Aliovalent ions can also be incorporated into the $ZrW_2O_8$ structure. Substitution of the Zr/Hf site by a number of trivalent ions (Sc, Y, In, Eu, Er, Yb, Lu) has been reported [77–81]. These systems show limited solubility, ranging from 1.6% for $Eu^{3+}$ to 5% for $Yb^{3+}$. However, even small amounts can lead to significant changes in $T_{trs}$. For example, 4% substitution lowers $T_{trs}$ to 390 K for $Y^{3+}$, 380 K for $In^{3+}$, and 360 K for $Sc^{3+}$ [80]. This clearly indicates that the trivalent substituents introduce disorder into the $ZrW_2O_8$ framework. Even at very low temperatures, only partial ordering is observed, similar to $ZrMoWO_8$. The phase transition temperature can be correlated to the normalized saturated order parameter η. All trivalent cations investigated are larger than $Zr^{4+}$ or $Hf^{4+}$. In addition, an oxygen vacancy is created for every two $A^{3+}$ cations, which is evident from the decrease of the lattice constant with increasing substitution by the larger cations. This results in a distortion of the $AO_6$ octahedra, which in turn act as a local, spherical disturbance on the bonded $MO_4$ tetrahedra. Yamamura et al. analyzed the anisotropic peak broadening observed for Sc, In and Y substituted $ZrW_2O_8$, and quantified the size of the distorted region as 1.3 to 1.7 nm, which is equivalent to 8 to 12 $WO_4$ units [80]. The expansion behavior in the disordered high temperature phase was identical to β-$ZrW_2O_8$, regardless of identity and quantity of substituent, while slightly less negative expansion was observed with increasing $A^{3+}$ content in the α-phase.

The only example of aliovalent substitution of the M site to date is the compound $ZrV_{0.2}W_{1.8}O_{7.9}$ [82,83]. This material was reported to crystallize in space group $Pa\bar{3}$, which is also adopted by both β-$ZrW_2O_8$ and $ZrV_2O_7$. The main difference between these structures lies in the fact that the $V_2O_7$ groups in $ZrV_2O_7$ are truly centrosymmetric, while the $W_2O_8$ groups are not, requiring equal amounts of opposite orientations to give an average centrosymmetric structure. A later publication on the same composition assigned space group $P2_13$ at room temperature, and reported a transition to the $Pa\bar{3}$ polymorph between 358 and 400 K. Interestingly, the β-phase expansion is less negative ($-1.6 \times 10^{-6}$ $K^{-1}$) than for most compositions ($-5 \times 10^{-6}$ $K^{-1}$), while the α-phase expansion is identical to $ZrW_2O_8$. The solubility limit of vanadium in $ZrW_2O_8$ has not yet been determined.

### 2.1.2. High Pressure Behavior

Open framework compounds are prone to undergo pressure-induced phase transitions. As the preparation and use of composites is likely to expose NTE fillers to pressure, their application requires investigation of their high pressure behavior. *In situ* experiments and measurements on samples recovered from high pressure have been reported for $ZrW_2O_8$ [4,7,84–87], $HfW_2O_8$ [63,88,89], $ZrMo_2O_8$ [54,90–92], and $HfMo_2O_8$ [90], but no solid solutions have been studied under pressure to date.

Cubic $ZrW_2O_8$ undergoes an irreversible phase transition to γ-$ZrW_2O_8$ at 0.2 to 0.3 GPa (Figure 4), which is accompanied by a 5% decrease in volume per formula unit. The structure of this phase is closely related to the α-polymorph, and involves a reorientation of one third of the $W_2O_8$ units, which results in tripling of one cell axis and lowering of the symmetry to the orthorhombic system [93]. γ-$ZrW_2O_8$ can be quenched to ambient conditions, and converts back to the cubic structure upon heating to 390 K. It shows weak NTE below 225 K, and positive expansion at higher temperatures.

Further compression of $ZrW_2O_8$ results in pressure-induced amorphization between 1.9 and 2.4 GPa [7]. The amorphous phase is ~25% denser than the cubic starting material, and can be retained upon decompression. To recrystallize α-$ZrW_2O_8$ at ambient pressure, heating to 923 K is necessary. Both pressure-induced phase transitions are accompanied by an increase in tungsten coordination: The orthorhombic unit cell contains one 4-coordinated W, four W atoms in 4 + 1 coordination, and one W with a 5 + 1 environment. Further changes in W coordination towards more centrosymmetric environments have been observed in PDF and XANES/EXAFS experiments during amorphization [87,94]. Zr K-edge EXAFS data on samples recovered after compression also suggest that the Zr coordination number may increase to 7 at higher pressures. These observations are consistent with a mechanism of amorphization that involves disordering of existing structural polyhedra, which leads to formation of additional bonds that crosslink the polyhedra and increase the metal coordination.

$HfW_2O_8$ shows very similar behavior to $ZrW_2O_8$, except that the transition to the γ-polymorph occurs at higher pressure (0.63 GPa) and shows sluggish kinetics [89]. Full conversion is only achieved after 24 h at 0.63 GPa, while no transformation occurs even after 11 d at 0.52 GPa. Amorphization is observed at ~2 GPa. Both γ- and amorphous $HfW_2O_8$ are metastable under ambient conditions. The orthorhombic material can be converted back to the cubic phase by heating to 360 K. No reports are available on the recrystallization of amorphous $HfW_2O_8$.

**Figure 4.** Compressibility of cubic $ZrW_2O_8$ (circles) and cubic $ZrMo_2O_8$ (diamonds) under hydrostatic conditions. Open symbols: Data collected upon compression; solid symbols: Data collected upon decompression.

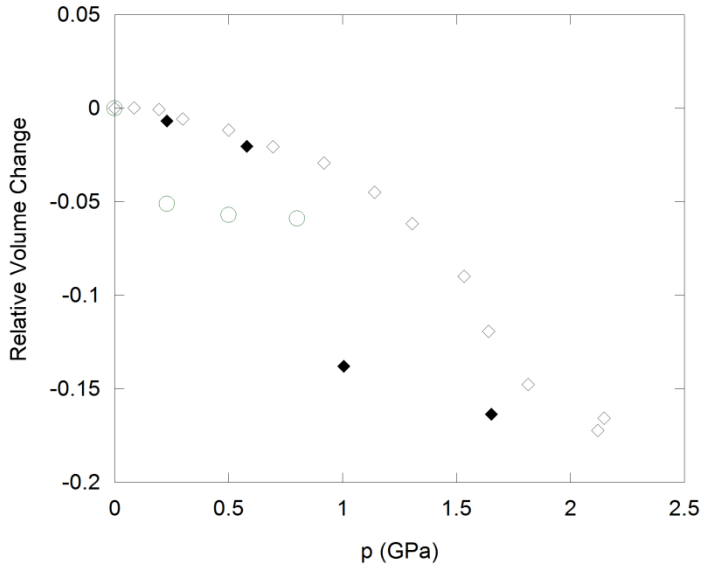


$ZrMo_2O_8$ and $HfMo_2O_8$ also undergo pressure-induced amorphization, and EXAFS/XANES studies on $ZrMo_2O_8$ suggest that the amorphous phase possesses similar local structures to $ZrW_2O_8$ [92]. The amorphous materials cannot be reconverted to the cubic structures. Instead, the more stable trigonal and monoclinic $AM_2O_8$ polymorphs are formed during heating at low and high pressure, respectively. Application of non-hydrostatic pressure results in amorphization at 0.5 to 1.5 GPa, while crystallinity is retained under hydrostatic conditions up to 3.0 GPa [90]. In hydrostatic environments, a crystalline-to-crystalline transition at 0.7–2.0 GPa precedes amorphization. This transformation is

accompanied by a 10–11% decrease in cell volume (Figure 4), suggesting that the still unknown structure of the high pressure polymorph is different from γ-$ZrW_2O_8$. The data could be fitted in a pseudo-cubic cell, although subtle peak splitting indicative of symmetry lowering was evident. The transition is reversible upon decompression, although considerable hysteresis is observed, with the original cubic phases reforming below 1.0 GPa.

### *2.2. $ZrV_2O_7$ Family*

Negative thermal expansion in the zirconium vanadate family was first reported in the mid 90's [1]. $ZrV_2O_7$ is thermodynamically stable up to ~1075 K, where decomposition into binary oxides is observed. Like $ZrW_2O_8$, $ZrV_2O_7$ adopts a cubic structure, making its expansion behavior inherently isotropic. The ideal $ZrV_2O_7$ structure is closely related to the rocksalt structure, with $Zr^{4+}$ as the cation, and $(V_2O_7)^{4-}$ as the anion. The $V_2O_7$ groups order along the threefold rotation axis, lowering the overall symmetry to $Pa\bar{3}$, and constraining the V-O-V bond angles to be linear on average, although significant displacements of the oxygen atoms from the inversion centers have been reported. The cations are octahedrally coordinated by oxygen, and the octahedra and tetrahedra form a corner-sharing 3D network (Figure 3b). This structural arrangement can give rise to transverse vibrations of corner-sharing oxygen atoms, which may result in NTE. In contrast to $ZrW_2O_8$, such vibrational modes always involve distortions of the polyhedra. The vibrations can thus not be described by the RUM model, but may be regarded as "quasi-rigid unit modes", or qRUMs [59]. $ZrV_2O_7$ shows strong NTE with $\alpha_l$ values between $-7$ and $-10 \times 10^{-6}$ $K^{-1}$ above 375 K, but undergoes phase transitions to an incommensurate phase, and to an ordered cubic $3 \times 3 \times 3$ superstructure in space group $Pa\bar{3}$ upon cooling to 375 and 350 K, respectively. In the room temperature superstructure, 2/3 of the V-O-V linkages are no longer constrained to be linear on average by symmetry, and the expansion coefficient becomes positive [95–97].

#### 2.2.1. Substitution of $ZrV_2O_7$

The $ZrV_2O_7$ structure can accommodate a wide range of tetra- and pentavalent ions. For M = P, the $A^{4+}$ cation can be Zr, Hf, Ti, U, Th, Pu, Np, Mo, W, Ce, Pb, Sn, Ge or Si [1], while for the vanadates only the Zr and Hf compounds [1], and for the arsenates only the Zr and Th compounds are known [98,99]. For a number of years, all compounds in the $AM_2O_7$ family were believed to adopt the ideal $ZrV_2O_7$ structure in space group $Pa\bar{3}$ at high temperatures, and to transform to the cubic $3 \times 3 \times 3$ superstructure at lower temperatures. This view has been challenged over the past decade. While $SiP_2O_7$, $TiP_2O_7$, and $HfV_2O_7$ indeed adopt a cubic $3 \times 3 \times 3$ superstructure, NMR and high resolution synchrotron studies have shown that the symmetry is lower for many materials. For example, $SnP_2O_7$ and $GeP_2O_7$ were found to be monoclinic [100–102], $CeP_2O_7$ and $AnP_2O_7$ (An = U, Th, Pu, Np) were reported as triclinic [103,104], and $ZrP_2O_7$ and $HfP_2O_7$ exhibit an orthorhombic distortion [105,106]. The structure of the latter compounds was solved independently from synchrotron single crystal and powder diffraction data by the Birkedal and Evans groups, and consists of a 136 atom unit cell in space group Pbca. All P-O-P bond angles are significantly smaller than 180°, eliminating the possibility of transverse oxygen vibrations that could lead to a unit cell contraction [105,106]. However, high resolution studies of $AnP_2O_7$ have shown that NTE can be observed at high temperature in materials

with bent P-O-P units [104]. Interestingly, $SnP_2O_7$ does not adopt the ideal $ZrV_2O_7$ structure at all, but undergoes a series of different distortions up to its decomposition temperature. Insufficient data are available to unambiguously address whether other $AM_2O_7$ compounds undergo symmetry-lowering distortions.

The magnitude of expansion of $AM_2O_7$ compounds depends on the identity of the A and M cations, which determine the size of the polyhedra. Larger polyhedra can accommodate the distortions required for transverse oxygen vibrations more easily, and as a result, most phosphates show positive expansion at all temperatures, while the vanadates show strong NTE in the high temperature phase. Phosphates with large $A^{4+}$ cations ($CeP_2O_7$, $AnP_2O_7$) show a change from positive to negative expansion with increasing temperature.

The phase transition temperature for the ideal $ZrV_2O_7$ can be suppressed by formation of solid solutions $Zr_{1-x}Hf_xV_{2-y}P_yO_7$ [1] While substitution of Hf for Zr has a limited effect on the phase transition temperature, the incorporation of P on the M site strongly influences the phase transition behavior. For small amounts of mixing, the transition temperatures for both phase changes are lowered, and for values of $0.4 < y < 1.6$, the materials adopt the high temperature $ZrV_2O_7$ structure at room temperature. Expansion coefficients range from small positive to strongly negative depending on composition.

Reports of substitution of the $ZrV_2O_7$ structure by aliovalent cations are rare, and are limited to formation of $A_{0.5}^{3+}A'_{0.5}^{5+}P_2O_7$ (A = Bi, Nb, Nd, Eu, Al, Fe, Ga, In, Y; A' = Nb, Ta) [107,108], $Nb_{0.05}Y_{0.05}Zr_{0.9}P_{2-x}V_xO_7$ [109], and $ZrV_{2-x}Mo_xO_{7+x/2}$ ($0 \leq x \leq 0.8$) [110]. Positive expansion was observed at all temperatures for the phosphates. The incorporation of $Y^{3+}$ and $Nb^{5+}$ into $ZrP_{2-x}V_xO_7$ reduced the positive expansion in the low temperature superstructure, but did not significantly alter the phase transition temperature and magnitude of NTE in the high temperature phase. Similarly to V-substituted $ZrW_2O_8$, the Mo-substituted $ZrV_2O_7$ crystallizes in space group $Pa\bar{3}$, and the structure is closely related to the $ZrMo_2O_8$ and $ZrV_2O_7$ parent structures. The expansion behavior determined for a single crystal with 25% Mo substitution is similar to that of $ZrV_2O_7$.

### 2.2.2. High Pressure Behavior

High pressure studies in the $ZrV_2O_7$ family have been limited to $TiP_2O_7$, $ZrP_2O_7$, $CeP_2O_7$, $ZrV_2O_7$ and $HfV_2O_7$ [103,111–114]. Interestingly, *in situ* diffraction experiments show no evidence for pressure-induced phase transitions or amorphization for $TiP_2O_7$ and $ZrP_2O_7$, both of which are positive thermal expansion compounds. Raman studies suggest that subtle structural changes could be occurring upon compression, but cell volumes extracted from X-ray data showed smooth compression up to 40 and 20 GPa, respectively [111].

In contrast, $CeP_2O_7$, $ZrV_2O_7$ and $HfV_2O_7$ undergo phase transitions to crystalline high pressure phases at 0.65 GPa, 1.6 GPa and 3.7 GPa. Peak splitting indicates lowering of the cubic symmetry in all cases. For $CeP_2O_7$, a second crystalline high pressure phase is observed above 5 GPa, while pressure-induced amorphization occurs above 4.0 GPa for $ZrV_2O_7$. $HfV_2O_7$ also progressively amorphizes, but traces of crystallinity are still observed at 42 GPa. Both transitions in $CeP_2O_7$ are reversible upon decompression. Raman studies on the vanadates suggest that amorphization is

irreversible, whereas the crystalline high pressure phase reverts back to the ambient pressure polymorph upon decompression.

### *2.3. $Sc_2W_3O_{12}$ Family*

The scandium tungstate family has also attracted a lot of attention, as it offers a wide range of possible compositions, and the potential to tune the expansion behavior of the resulting compounds [5,23]. $Sc_2W_3O_{12}$ is thermodynamically stable over a wide temperature range, allowing straightforward preparation by traditional ceramic methods. Unlike $ZrW_2O_8$ and $ZrV_2O_7$, it does not adopt a cubic structure, but crystallizes in the orthorhombic space group Pnca [115]. This gives rise to anisotropic expansion. The crystal structure is composed of a corner-sharing network of $ScO_6$ octahedra and $WO_4$ tetrahedra (Figure 5a). Negative volume expansion is observed from 10 to 1300 K [115,116], and an average $\alpha_l$ value of $-2.2 \times 10^{-6}$ $K^{-1}$ was determined from variable diffraction data for the range 50–450 K. Dilatometry on ceramic bars gave significantly more negative values of $-6$ to $-11 \times 10^{-6}$ $K^{-1}$ which was attributed to the presence of microcracks in the bars combined with the anisotropic expansion of the three unit cell axes, where the a and c axis contract, while the b axis expands. Detailed structural analysis showed that there were only small changes in bond distances and angles within the polyhedra as a function of temperature, but large amplitudes of vibration were observed for the corner-sharing oxygen atoms. While later theoretical studies showed that no true RUMs are present in the structure [59], the atomic displacement parameters extracted from diffraction data clearly demonstrate that transverse oxygen vibrations give rise to the observed NTE. While $Sc_2W_3O_{12}$ remains orthorhombic at all temperatures, other compounds in this family undergo a symmetry-lowering displacive phase transition to a denser monoclinic polymorph at low temperatures (Figure 5b). In general, the orthorhombic $Sc_2W_3O_{12}$ structure is classified as an NTE polymorph, while positive expansion has been reported for monoclinic phases.

**Figure 5.** Crystal structures of (**a**) orthorhombic; (**b**) monoclinic $Al_2Mo_3O_{12}$; bright: $AlO_6$ octahedra; dark: $MoO_4$ tetrahedra.

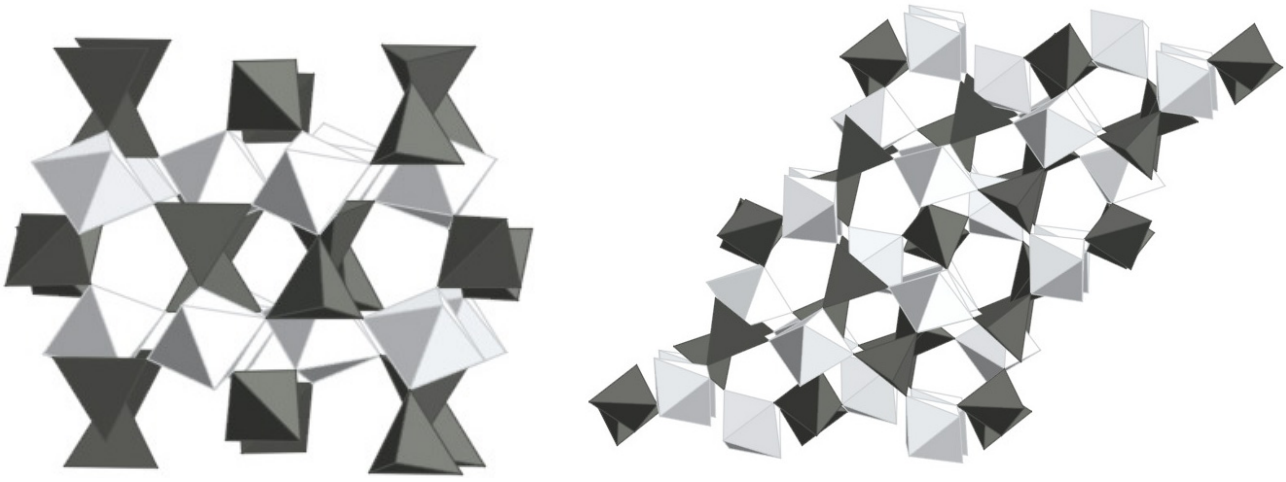

(**a**) (**b**)

The phonon density of state (DOS) for $Sc_2W_3O_{12}$ has been determined from specific heat measurements. Like for $ZrW_2O_8$, very low energy phonons (~5 meV) with negative $\gamma_i$ values, and a gap between the low and high energy phonons were observed [21]. Interestingly, a similar DOS distribution was found for $Sc_2Mo_3O_{12}$, which adopts a monoclinic structure at low temperature. This suggests that the monoclinic structure has the potential to exhibit NTE as well. While the higher energy phonon contributions with positive $\gamma_i$ values outweigh the effect of the low energy phonons with negative Grüneisen parameters at most temperatures, negative expansion of the b axis (4–60 K) and very small negative volume expansion (4–30 K, $\alpha_v = -3.7 \times 10^{-7}$ K$^{-1}$) were observed at very low temperatures [117].

### 2.3.1. Substitution of $Sc_2W_3O_{12}$

The scandium tungstate structure shows excellent tolerance towards ionic substitution of both metal sites. In most $A_2M_3O_{12}$ compounds, the M site is occupied by Mo or W. In these cases, the A site can be substituted by any trivalent cation ranging in size from $Al^{3+}$ ($r_{oct}$ = 0.54 Å) to $Ho^{3+}$ ($r_{oct}$ = 0.90 Å). $Ln_2M_3O_{12}$ compositions with larger lanthanides crystallize in structures that adopt higher coordination numbers (7 or 8) for the A-site. However, for solid solutions of two trivalent cations, significant amounts of larger $Ln^{3+}$ can be incorporated into the scandium tungstate structure, as evidenced by reports of $Er_{2-x}Ce_xW_3O_{12}$ ($x \leq 0.4$) [118], $Er_{2-x}Sm_xW_3O_{12}$ ($x \leq 0.5$) [119], $Er_{2-x}Nd_xW_3O_{12}$ ($x \leq 0.5$) [120], $Er_{2-x}Dy_xW_3O_{12}$ ($x \leq 0.7$) [121], $Y_{2-x}Dy_xW_3O_{12}$ ($x \leq 1.0$) [121], and $Y_{2-x}Nd_xW_3O_{12}$ ($x \leq 0.4$) [122]. In addition, substitution with aliovalent cations has been achieved in $AP_2MO_{12}$ [123,124] and $MgAM_3O_{12}$ (A = Zr, Hf; M = Mo, W) [125–127]. $AP_2MO_{12}$ adopts the same structure as $Sc_2W_3O_{12}$ with an ordered arrangement of P and M [124], while $MgAM_3O_{12}$ crystallizes in a different orthorhombic structure in space group Pnma or $Pna2_1$ [125,126].

Many $A_2M_3O_{12}$ compositions adopt a monoclinic structure at low temperatures, and transform to the orthorhombic Pnca phase upon heating [117]. The temperature for this phase transition is generally higher for molybdates than for tungstates, and increases with increasing electronegativity of the A-site cation [128]. This observation can be explained by the fact that oxygen-oxygen repulsive interactions make the denser monoclinic phase less favorable. More electronegative A-site elements reduce the partial charge on the oxygen atoms and thus the repulsive forces. However, shifts in the temperature or the complete absence of the phase transition for some mixed A-site compounds suggest that entropic factors also play a role. As the monoclinic phase generally displays positive expansion, this phase transition is undesirable for any potential uses of these NTE compounds in composites.

The expansion coefficient of the orthorhombic phase depends strongly on the identity of the A-site cation. As stated earlier, the $A_2M_3O_{12}$ structure does not support RUMs, and distortion of the polyhedra occurs during the transverse vibrations of oxygen atoms. Larger A-site cations give rise to softer octahedra that distort more easily. As a result, expansion tends to become more negative with increasing size of $A^{3+}$, reaching values of $-7.0 \times 10^{-6}$ K$^{-1}$ in $Y_2W_3O_{12}$ [129] and $-9.3 \times 10^{-6}$ K$^{-1}$ in $Y_2Mo_3O_{12}$. Additional slight decreases have been achieved in solid solutions of these compounds with larger lanthanides [118–122]. In contrast, $Al_2W_3O_{12}$ has been reported to show low positive expansion with an $\alpha_l$ value of $+2.2 \times 10^{-6}$ K$^{-1}$ [5]. Reports on expansion coefficients vary not only between $\alpha_l$ values extracted from variable temperature diffraction data and dilatometry, but also between different

diffraction measurements. These discrepancies may in some cases arise from averaging over different temperature ranges, as the volume expansion of many $A_2M_3O_{12}$ compounds is not completely linear. Nevertheless, the accumulated knowledge on the expansion behavior of different compositions can be used to design materials with desired α values, including zero expansion compounds. The first report of a solid solution with close to zero expansion around room temperature ($InAlW_3O_{12}$) was published in 1999 by Mary and Sleight [23]. More sophisticated solid solutions like $Al_{2x}(MgHf)_{1-x}W_3O_{12}$ have since been reported [130].

While the record negative expansion coefficients in the $A_2M_3O_{12}$ family have been achieved with rare earth elements or the "pseudo-lanthanide" Y, it is necessary to point out that all of these compositions suffer from hygroscopicity. Under ambient conditions, a trihydrate is formed by absorption of moisture from the atmosphere [118–122,131,132]. This limits the usefulness of these compositions to temperatures above the dehydration point or sealed systems. In addition, several of these compounds could be on the borderline of thermodynamic stability of the Pnca-NTE polymorph, as it was shown that this structure is only thermodynamically stable above 823 K for $Y_2Mo_3O_{12}$, and metastable with respect to a denser Pba2-polymorph at lower temperatures [133] (Figure 6).

**Figure 6.** Crystal structures of (**a**) Pba2-$Y_2Mo_3O_{12}$; (**b**) Pbcn-$Y_2Mo_3O_{12}$; bright: $YO_n$ polyhedral; dark: $MoO_4$ tetrahedra. In the denser Pba2 polymorph, the coordination number of yttrium is increased, and the polyhedra share edges.

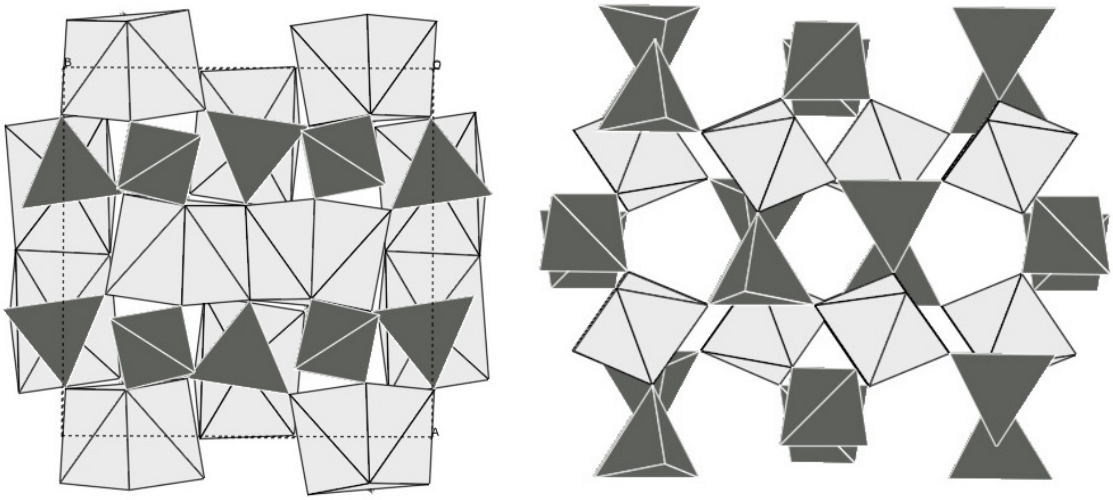

(**a**) (**b**)

2.3.2. High Pressure Behavior

A number of $A_2M_3O_{12}$ materials have been studied under pressure by diffraction and spectroscopic methods. Orthorhombic compounds tend to undergo a transition to the denser monoclinic polymorph at very low pressures (<0.6 GPa) [134–138]. Most compounds investigated *in situ* undergo at least one additional crystalline-to-crystalline phase transition [135,137–147]. Pressure-induced amorphization is observed at pressures ranging from 5 GPa to 20 GPa. Similar high pressure diffraction patterns were observed for $Sc_2W_3O_{12}$ [136], $Sc_2Mo_3O_{12}$ [135], $Al_2W_3O_{12}$ [143], and $Ga_2Mo_3O_{12}$ [146], but due to limited data quality, the structures have not been characterized.

### *2.4. Other NTE Oxides*

In addition to the $ZrW_2O_8$, $ZrV_2O_7$ and $Sc_2W_3O_{12}$ families discussed so far, NTE due to transverse atomic vibrations has been observed in several other oxide structures. Many zeolites and zeolitic frameworks (AlPOs, GaPOs) exhibit this unusual property, which is not surprising considering that their structures are composed of corner-sharing tetrahedral networks [24,148]. In "normal" zeolites that contain a mixture of Si and Al, the presence of counter ions and water interferes with NTE, as the amount of empty space is reduced. This makes pure siliceous zeolites and group 13 phosphates better targets for studying NTE in zeolites. The magnitudes of NTE differ widely from close to zero in chabazite to the record of $\alpha_l = -11.7 \times 10^{-6}$ $K^{-1}$ in AlPO-17 [24,55,149] (Figure 7).

**Figure 7.** Crystal structures of (**a**) chabazite; (**b**) AlPO-17.

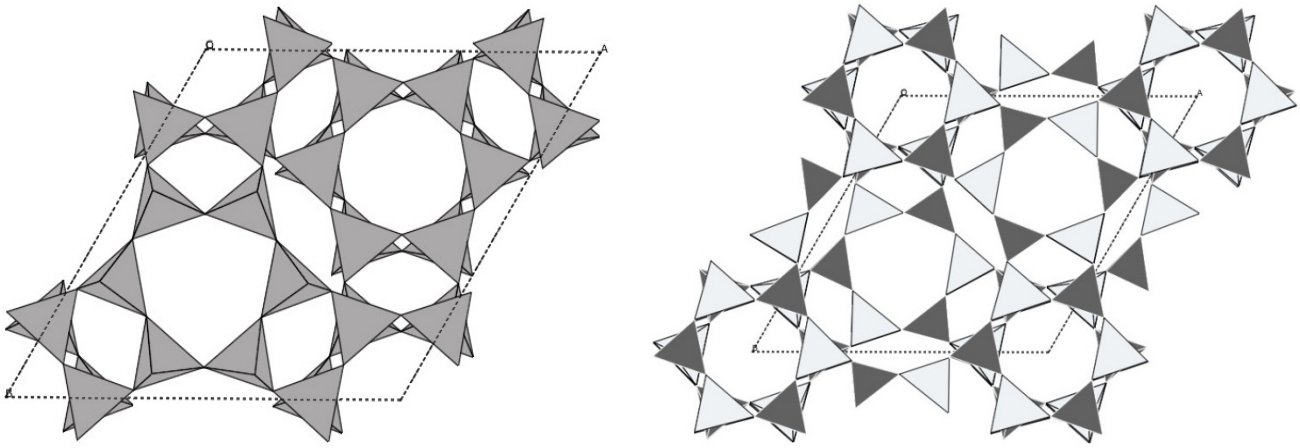

(**a**) (**b**)

Another interesting example is found in $Ag_2O$ and $Cu_2O$, in which the cations are linearly coordinated by two oxygens, and occupy the corners of the tetrahedral network of $OM_4$ units. The overall structure consists of two independent, interpenetrating $OM_4$ networks. NTE in $Cu_2O$ at low temperatures was first reported in 1985 [150], while this behavior was only documented in $Ag_2O$ in 2002 [13] EXAFS studies indicate significant distortion of the $OM_4$ units, showing that a RUM model is not adequate to describe their expansion behavior [13,151]. A recent PDF study suggests that the distortion can lead to a shortening of the tetrahedral edge length and thus contribute to the NTE arising from transverse vibrations [43].

NTE has also been reported in materials with the delafossite structure [152–154], $A^{IV}{}_2O(PO_4)_2$ (A = Zr, Hf, U, Th) [155–159], $ReO_3$ [160], $NbOPO_4$ [161–163], $NbVO_5$ [164], and $TaVO_5$ [165]. While not an oxide, strong NTE in $ScF_3$, which adopts the simple $ReO_3$ structure, was reported by Greve *et al.* in 2010 [166]. This compound constitutes the first example of NTE over a wide temperature range in a purely octahedral framework.

### *2.5. Metal Cyanide Networks*

Negative thermal expansion in metal cyanide frameworks was first reported for $Zn(CN)_2$ by Williams *et al.* in 1997 [167]. This compound adopts a purely tetrahedral framework similar to

silicates, but instead of a corner-sharing oxygen, the tetrahedra are connected by a diatomic cyanide linker. $Fe[Co(CN)_6]$ was the first purely octahedral metal cyanide network reported to display NTE in 2004 [58]. Its structure is related to the $ReO_3$ structure by replacing the corner-sharing oxygen atoms of the octahedra by a diatomic cyanide bridge. Such frameworks can accommodate the same polyhedral rocking motions that cause NTE in the oxide families discussed so far, but the diatomic bridges give the structures more flexibility, which favors low frequency vibrational modes and increases the number of possible RUMs [168] The transverse vibrations of the CN linkers could be directly observed by pair distribution function analysis [15].

Metal cyanide frameworks quickly became the record holders for strongest NTE behavior with reports of $\alpha_l$ values as low as $-33 \times 10^{-6}$ $K^{-1}$ for $Cd(CN)_2$ [20], $-40 \times 10^{-6}$ $K^{-1}$ for $Zn_3[Fe(CN)_6]_2$, $Fe_3[Co(CN)_6]_2$ and $Co_3[Co(CN)_6]_2$ [169], and $-48 \times 10^{-6}$ $K^{-1}$ for $Mn_3[Co(CN)_6]_2$ [169]. It was also recognized that like in zeolites, the presence of guest molecules in the open frameworks interferes with the transverse vibrations of the linker groups, thus reducing the NTE coefficients [57]. Additional materials were synthesized, and composition dependent NTE was reported for a number of metal ions [18,170].

In 2008, metal cyanide networks set another record when colossal positive and negative (colossal: $|\alpha| \geq 100 \times 10^{-6}$ $K^{-1}$) expansion behavior was observed in $Ag_3[Co(CN)_6]$ along different unit cell axes [19]. The a axis of the trigonal unit cell expands with $+130 \times 10^{-6}$ $K^{-1} \leq \alpha_a \leq +150 \times 10^{-6}$ $K^{-1}$, while the c axis shows a similar magnitude of contraction with $-130 \times 10^{-6}$ $K^{-1} \leq \alpha_c \leq -120 \times 10^{-6}$ $K^{-1}$. Transverse vibrations of cyanide groups, which are observed in the structure, cannot account for the observed expansion behavior. The simultaneous observation of colossal positive and negative expansion points to the crystal structure as the source of this unusual behavior [171]. This material is composed of sheets of $Co(CN)_6$ octahedra that are separated by layers of $Ag^+$ ions. Each $Ag^+$ is linearly coordinated by two cyanide groups, one from each adjacent layer. Ag···Ag contacts close to the sum of van der Waals radii are observed, which suggest argentophilic interactions. These Ag···Ag and the corresponding $[Co(CN)_6]\cdots[Co(CN)_6]$ contacts increase rapidly with temperature. In order to preserve the Co-CN-Ag-NC-Co bridges in the material, the strong expansion along the a axis must be coupled to equally strong contraction along the c axis, which has been described as similar to "garden lattice fencing". It was later established that the argentophilic interactions between silver atoms are the major driving force for the observed colossal expansion behavior, as isostructural $D_3[Co(CN)_6]$ did not display colossal behavior [172]. However, strong metallophilic interactions can reduce expansion coefficients [44].

## 3. Composites

One of the reasons why NTE materials have attracted significant interest from the science and engineering communities lies in their potential applications as fillers in controlled thermal expansion composites. Mismatches in thermal expansion of device components have long been recognized as a serious problem, whether in the expansion of road surfaces, railroad tracks and bridges, or in thin films where lattice matching at deposition and use temperatures is important. Precision positioning is critical in electronic devices, and nanotechnology only amplifies the level of control necessary for proper function.

In most modern applications, very specific materials' properties are required, which may include conductivity, magnetic and optical properties, hardness, ductility or more. This can make it difficult to achieve zero expansion or match the expansion coefficient of another device component. In such cases, use of composites is an attractive alternative, which can allow preservation of desirable material properties while modifying unfavorable ones or adding new, advantageous ones. NTE materials can theoretically be used to reduce or offset the expansion of any other material through preparation of controlled thermal expansion composites. In practice, the preparation of high quality composites poses a number of interesting engineering challenges.

### *3.1. Desirable Properties of Filler Materials*

The best filler material for any controlled expansion composite is the least expensive compound that will achieve the desired reduction in expansion and can easily be prepared in the necessary quantities. In addition, stability under processing and use conditions, and compatibility with other system components, is necessary. *In situ* phase formation may aid in achieving homogeneous composites, alternatively, small particle sizes will improve mixing. Scaling up processes to industrial scale will likely bring additional challenges. Materials with isotropic NTE offer the advantage that filler particle orientation does not affect expansion, making isotropic behavior desirable in many cases. However, if the expansion of a highly oriented matrix or device needs to be compensated, anisotropic NTE may be preferable.

The exact optimum properties of a filler material can change depending on the exact nature of the composite. For example, compatibility will depend on the identity and properties of other device components. Similarly, the targeted application for a device will often dictate processing and conditions (temperature, pressure, atmosphere/environment *etc.*). Nevertheless, there are certain known properties of NTE materials that could impede their usefulness in controlled thermal expansion composites, which will be discussed in the following section.

### *3.2. Potential Problems with Known NTE Filler Materials*

With the exception of zeolitic materials, all NTE materials discussed in this review contain transition metals, which generally increases the price of the starting materials. For high end applications where other device components or manufacturing processes already have a significant cost, the added expense of small amounts of NTE materials becomes negligible. However, for mass production of cheaper devices, the NTE filler cost may prove prohibitive. Zr, V, Mo and W based starting materials are significantly more expensive than zeolites, and many $Sc_2W_3O_{12}$-type compounds that show NTE around room temperature contain expensive lanthanides or pseudo-lanthanides. Commercial availability is another important consideration. Zeolites are readily available, but $ZrW_2O_8$ is the only NTE material discussed in Sections 2.1 through 2.3 that can be purchased. The commercially available $ZrW_2O_8$ powder has a median particle size of 15-20 μm, and may contain small $ZrO_2$ and $WO_3$ impurities.

The ease of preparation of NTE fillers depends on their thermodynamic stability and whether particle size control is necessary. Most compounds in the $ZrV_2O_7$ and $Sc_2W_3O_{12}$ families are thermodynamically stable, and can be obtained by traditional ceramic methods [1,5]. In contrast, the

$ZrW_2O_8$-type materials are metastable at room temperature, requiring rapid quenching and thus limiting batch sizes for traditional solid state synthesis [34,71]. Preparation of significant quantities of $ZrMo_2O_8$ or $HfMo_2O_8$ by high temperature approaches may not be feasible. In addition, $P_2O_5$, $V_2O_5$, $MoO_3$ and $WO_3$ show considerable volatility at high temperatures, making extended heating of binary oxide starting mixtures unfavorable. Solution based routes to all families of NTE compounds have been reported, which offer the added advantage of particle size control [173,174]. However, synthesis conditions must be carefully optimized to ensure preparation of stoichiometric, homogeneous NTE compounds, especially for complex solid solutions. For the $ZrW_2O_8$ family, low temperature routes require topotactic recrystallization at a temperature where the compounds are metastable, which further complicates the preparation of phase pure samples, especially for the molybdates [69]. $AM_2O_8$ compounds and other NTE materials with an upper limit of thermal stability are not suitable for ceramic composites that require sintering at high temperature.

The temperature range over which a material displays NTE is important. For most applications, this range should include room temperature, and a wider range of NTE can be considered beneficial. This makes several zeolites, the $ZrV_2O_7$ family and $Sc_2W_3O_{12}$-type materials with smaller $A^{3+}$ cation less attractive.

A major drawback of many NTE materials is their instability under moderate pressure. Composite preparation has to avoid pressures at which the filler irreversibly transforms to a different phase. In addition, pressure-induced phase transitions can cause problems during thermal cycling of composites if localized pressures on individual filler particles exceed the transition pressure. $ZrW_2O_8$ and $HfW_2O_8$ show the most detrimental behavior in this respect, with irreversible phase transitions at 0.2 and 0.6 GPa, respectively [84,89]. While many orthorhombic $A_2M_3O_{12}$ compounds transform to a denser monoclinic phase at 0.3 to 0.7 GPa as well [135,136,143], this transition is reversible upon decompression. $Zr_2WP_2O_{12}$ transforms to the denser monoclinic polymorph as well, but only above 1.4 GPa [145].

Another problem arises from the instability of some NTE compounds under ambient conditions unless they are used in a sealed system. $A_2M_3O_{12}$ compositions are very hydroscopic when A is a lanthanide or yttrium, forming a trihydrate $A_2M_3O_{12}\cdot 3H_2O$ within minutes of exposure to atmospheric moisture. While the water can be removed by heating, repeated hydration and dehydration is likely to accelerate composite deterioration. Solid solutions $Zr_{1-x}Hf_xMo_{2-y}W_yO_8$ with 30 to 90% tungsten content also incorporate water into their crystal structures [175,176], although the absorption is slower and does not lead to a significant change in crystal structure. Recently, this autohydration behavior was also observed in nanosized $ZrW_2O_8$ [177], while micron sized particles required hydrothermal treatment at 180 °C to force water into the structure [175].

Lastly, compatibility and mixing of filler and matrix are important for the preparation of composites. While other components in ceramic composites are usually compatible with NTE fillers, reactivity towards metals has been reported [49], and poor interaction between as-prepared filler particles and matrix has been observed in polymer composites [178–180].

### *3.3. Literature Reports on Composites with NTE Fillers*

To date, literature reports on composites using the NTE fillers discussed in this review article are sparse. Zeolitic materials have not been utilized in attempts to reduce other materials' expansion, despite their commercial availability and lower cost. This may be related to the fact that their expansion behavior is strongly influenced by guest molecules, making their behavior in composites less predictable. Interestingly, the NTE observed in many zeolites has been reported as a problem, as their shrinkage leads to crack formation and delamination between zeolite membranes and alumina supports [181,182]. Recently, use of a zeolite-based support instead of alumina was proposed to overcome this expansion mismatch [183].

With two exceptions, NTE composite research has focused on $ZrW_2O_8$. A ceramic $Fe_xSc_{2-x}Mo_3O_{12}/MoO_3$ composite with close to zero thermal expansion was prepared by melt reaction [184]. The final composite contained significant void space and was brittle, which was attributed to evaporation of $MoO_3$. In addition, a magnesium composite containing 20 vol% $Zr_2WP_2O_{12}$ was reported [185]. The overall expansion coefficient was only slightly reduced.

$ZrW_2O_8$ has been incorporated into metal, ceramic and polymer composites. Most of the metal composite work focused on Cu composites [49,50,186–190]. Cu is used as a heat sink in microelectronics, and copper composites that match the expansion coefficient of Si ($4 \times 10^{-6}$ $K^{-1}$) or $Al_2O_3$ ($7 \times 10^{-6}$ $K^{-1}$) could find widespread applications [49]. However, in all cases, formation of significant amounts of orthorhombic γ-$ZrW_2O_8$ was observed during thermal cycling. It was found that the copper matrix exerts a pressure of ~0.45 GPa on the filler particles [187,189], which is high enough to induce the cubic to orthorhombic phase transition. Attempts to reduce the local stress through precoating of particles with Cu did not succeed in suppressing the transformation [190]. It should be possible to overcome this problem by using $HfW_2O_8$ as a filler instead of $ZrW_2O_8$, however, no such attempts have been reported to date. An exploratory investigation on a $ZrW_2O_8$/low expansion steel composite ($\alpha_{steel} = 1.5 \times 10^{-6}$ $K^{-1}$) still observed formation of γ-$ZrW_2O_8$, clearly indicating that the application of $ZrW_2O_8$ will be limited to environments that will not exert significant pressure on the filler particles [191].

The exploratory synthesis of $ZrW_2O_8/SiO_2$ [192] and $ZrW_2O_8$/cement composites [193] have been reported. However, most $ZrW_2O_8$/ceramic composites have used $ZrO_2$ [51,52,194–200] or $Zr_2WP_2O_{12}$ [201–203] as the second component. Due to the similarity of the two components, good compatibility was observed. Formation of dense ceramic bodies (up to 95% dense) was achieved by addition of small amounts of $Al_2O_3$ [194,195], and control of thermal expansion ranging from negative to positive values was achieved for $ZrO_2$, while all $ZrW_2O_8/Zr_2WP_2O_{12}$ mixtures exhibited negative expansion. The α- to β-transition of $ZrW_2O_8$ was suppressed for composites with 75% $Zr_2WP_2O_{12}$.

$ZrW_2O_8$ has been incorporated into several polymer systems, including phenolic resins [204], epoxy resins [205] and polyimides [178–180]. In contrast to oxide ceramics, $ZrW_2O_8$ is not readily compatible with most polymer systems, and surface modification of filler particles is necessary to achieve good interaction with the matrix [178,179,205]. Significant reductions in expansion have been observed in all cases, ranging from 30% reduction for phenolic resins with 52 vol% and polyimides with 22 vol% filler to 60% reduction in epoxy composites for 40 vol% loading. Significant particle agglomeration was observed when large filler particles were used. In addition, large particles are prone

to settling at the bottom of any polymer composite films during film formation. Nanoparticles can be used to overcome this problem [178,179], however, a compromise between particle size and kinetics of the recently reported autohydration [177] will have to be found. Optimization of processing conditions like the use of reprecipitation blending reported for polyimide composites may allow formation of homogeneous $ZrW_2O_8$/polymer composites with intermediate particle size [179].

## 4. Conclusions

Negative thermal expansion has been established as a specialized field of research since the mid 1990s. New materials belonging to previously identified families of compounds, new families of NTE materials, and new insights into mechanisms are added to the literature every year. The initially predicted widespread use of NTE materials as fillers in a variety of controlled thermal expansion composites has not yet been achieved, but some promising preliminary results on $ZrW_2O_8/ZrO_2$ and $ZrW_2O_8$/polymer systems have been reported. Exploration of other filler materials that are less pressure sensitive or do not autohydrate under ambient conditions will be necessary to further the applications of NTE fillers, and will likely lead to interesting application as the field matures.

## Acknowledgments

Some of the work presented in this review was supported by the National Science Foundation under grant DMR-0545517.

## References and Notes

1. Korthuis, V.; Khosrovani, N.; Sleight, A.W.; Roberts, N.; Dupree, R.; Warren, W.W. Negative thermal expansion and phase transitions in the $ZrV_{2-x}P_xO_7$ series. *Chem. Mater.***1995**, *7*, 412–417.
2. Sleight, A.W. Thermal Contraction. *Endeavour* **1995**, *19*, 64–68.
3. Mary, T.A.; Evans, J.S.O.; Vogt, T.; Sleight, A.W. Negative thermal expansion from 0.3 to 1050 Kelvin in $ZrW_2O_8$. *Science* **1996**, *272*, 90–92.
4. Evans, J.S.O.; Hu, Z.; Jorgensen, J.D.; Argyriou, D.N.; Short, S.; Sleight, A.W. Compressibility, phase transitions, and oxygen migration in zirconium tungstate, $ZrW_2O_8$. *Science* **1997**, *275*, 61–65.
5. Evans, J.S.O.; Mary, T.A.; Sleight, A.W. Negative thermal expansion in a large molybdate and tungstate family. *J.Solid State Chem.* **1997**, *133*, 580–583.
6. Ernst, G.; Broholm, C.; Kowach, G.R.; Ramirez, A.P. Phonon density of states and negative thermal expansion in $ZrW_2O_8$. *Nature* **1998**, *396*, 147–149.
7. Perottoni, C.A.; da Jornada, J.A.H. Pressure-induced amorphization and negative thermal expansion in $ZrW_2O_8$. *Science* **1998**, *280*, 886–889.
8. Ramirez, A.P.; Kowach, G.R. Large low temperature specific heat in the negative thermal expansion compound $ZrW_2O_8$. *Phys. Rev. Lett.* **1998**, *80*, 4903–4906.
9. Sleight, A.W. Negative thermal expansion materials. *Curr. Opin. Solid State Mater. Sci.* **1998**, *3*, 128–131.

10. Ravindran, T.R.; Arora, A.K.; Mary, T.A. High pressure behavior of $ZrW_2O_8$: Gruneisen parameter and thermal properties. *Phys. Rev. Lett.* **2000**, *84*, 3879–3882.
11. Reisner, B.A.; Lee, Y.; Hanson, J.C.; Jones, G.A.; Parise, J.B.; Corbin, D.R.; Toby, B.H.; Freitag, A.; Larese, J.Z.; Kahlenberg, V. Understanding negative thermal expansion and 'trap door' cation relocations in zeolite rho. *Chem. Commun.* **2000**, *22*, 2221–2222.
12. Mittal, R.; Chaplot, S.L.; Schober, H.; Mary, T.A. Origin of negative thermal expansion in cubic $ZrW_2O_8$ revealed by high pressure inelastic neutron scattering. *Phys. Rev. Lett.* **2001**, *86*, 4692–4695.
13. Beccara, S.A.; Dalba, G.; Fornasini, P.; Grisenti, R.; Sanson, A. Local thermal expansion in a cuprite structure: The case of $Ag_2O$. *Phys. Rev. Lett.* **2002**, *89*, 025503:1–025503:4.
14. Birkedal, H.; Schwarzenbach, D.; Pattison, P. Observation of uniaxial negative thermal expansion in an organic crystal. *Angew. Chem.* **2002**, *114*, 780–782.
15. Chapman, K.W.; Chupas, P.J.; Kepert, C.J. Direct observation of a transverse vibrational mechanism for negative thermal expansion in $Zn(CN)_2$: An atomic pair distribution function analysis. *J. Am. Chem. Soc.* **2005**, *127*, 15630–15636.
16. Huang, L.P.; Kieffer, J. Structural origin of negative thermal expansion in high-temperature silica polymorphs. *Phys. Rev. Lett.* **2005**, *95*, 215901:1–215901:4.
17. Tucker, M.G.; Goodwin, A.L.; Dove, M.T.; Keen, D.A.; Wells, S.A.; Evans, J.S.O. Negative thermal expansion in $ZrW_2O_8$: Mechanisms, rigid unit modes, and neutron total scattering. *Phys. Rev. Lett.* **2005**, *95*, 255501:1–255501:4.
18. Chapman, K.W.; Chupas, P.J.; Kepert, C.J. Compositional dependence of negative thermal expansion in the Prussian blue analogues $(MPt^{IV})$-$Pt^{II}(CN)_6$ (M = Mn, Fe, Co, Ni, Cu, Zn, Cd). *J. Am. Chem. Soc.* **2006**, *128*, 7009–7014.
19. Goodwin, A.L.; Calleja, M.; Conterio, M.J.; Dove, M.T.; Evans, J.S.O.; Keen, D.A.; Peters, L.; Tucker, M.G. Colossal positive and negative thermal expansion in the framework material $Ag_3[Co(CN)_6]$. *Science* **2008**, *319*, 794–797.
20. Phillips, A.E.; Goodwin, A.L.; Halder, G.J.; Southon, P.D.; Kepert, C.J. Nanoporosity and exceptional negative thermal expansion in single-network cadmium cyanide. *Angew. Chem.* **2008**, *120*, 1418–1421.
21. Yamamura, Y.; Ikeuchi, S.; Saito, K. Characteristic Phonon spectrum of negative thermal expansion materials with framework structure through calorimetric study of $Sc_2M_3O_{12}$ (M = W and Mo). *Chem. Mater.* **2009**, *21*, 3008–3016.
22. Azuma, M.; Chen, W.T.; Seki, H.; Czapski, M.; Olga, S.; Oka, K.; Mizumaki, M.; Watanuki, T.; Ishimatsu, N.; Kawamura, N.; Ishiwata, S.; Tucker, M.G.; Shimakawa, Y.; Attfield, J.P. Colossal negative thermal expansion in $BiNiO_3$ induced by intermetallic charge transfer. *Nature Commun.* **2011**, *2*, doi: 10.1038/ncomms1361.
23. Mary, T.A.; Sleight, A.W. Bulk thermal expansion for tungstate and molybdates of the type $A_2M_3O_{12}$. *J. Mater. Res.* **1999**, *14*, 912–915.
24. Lightfoot, P.; Woodcock, D.A.; Maple, M.J.; Villaescusa, L.A.; Wright, P.A. The widespread occurrence of negative thermal expansion in zeolites. *J. Mater. Chem.* **2001**, *11*, 212–216.
25. *Negative or Zero Thermal Expansion Materials* (Special Issue Name); Journal of the Chinese Ceramic Society: Beijing, China, 2009; Volume 37, pp. 651–759.

26. Scheel, K. Versuche ueber die ausdehnung fester koerper, insbesondere von quarz in richtung der hauptachse, platin, palladium und quarzglas bei der temperatur der fluessigen Luft. *Verh. Deutsch. Phys. Ges.* **1907**, *9*, 3–23.
27. Scheel, K. Ueber die ausdehnung des quarzglases. *Verh. Deutsch. Phys. Ges.* **1907**, *9*, 719–721.
28. Hummel, F.A. Thermal expansion properties of natural Lithia minerals. *Foote Prints* **1948**, *20*, 3–11.
29. Hummel, F.A. Termal expansion properties of some synthetic lithia minerals. *J. Am. Ceram. Soc.* **1951**, *34*, 235–239.
30. Roy, R.; Agrawal, D.K.; McKinstry, H.A. Very low thermal expansion coefficient materials. *Annu. Rev. Mater. Sci.* **1989**, *19*, 59–81.
31. Boilot, J.P.; Salanie, J.P. Phase transformation in $Na_{1+x}Si_xZr_2P_{3-x}O_{12}$ compounds. *Mater. Res. Bull.* **1979**, *14*, 1469–1477.
32. Limaye, S.Y.; Agrawal, D.K.; Roy, R.; Mehrotra, Y. Synthesis, sintering and thermal-expansion of $Ca_{1-x}Sr_xZr_4P_6O_{24}$—An ultra-low thermal-expansion ceramic system. *J. Mater. Sci.* **1991**, *26*, 93–98.
33. Lenain, G.E.; McKinstry, H.A.; Alamo, J.; Agrawal, D.K. Structural model for thermal expansion in $MZr_2P_3O_{12}$ (M = Li, Na, K, Rb, Cs). *J. Mater. Sci.* **1987**, *22*, 17–22.
34. Graham, J.; Wadsley, A.D.; Weymouth, J.H.; Williams, L.S. A new ternary oxide, $ZrW_2O_8$. *J. Am. Ceram. Soc.* **1959**, *42*, 570.
35. Martinek, C.; Hummel, F.A. Linear thermal expansion of three tungstates. *J. Am. Ceram. Soc.* **1968**, *51*, 227–228.
36. Pryde, A.K.A.; Hammonds, K.D.; Dove, M.T.; Heine, V.; Gale, J.D.; Warren, M.C. Origin of the negative thermal expansion in $ZrW_2O_8$ and $ZrV_2O_7$. *J. Phys. Condens. Matter* **1996**, *8*, 10973–10982.
37. Pryde, A.K.A.; Hammonds, K.D.; Dove, M.T.; Heine, V.; Gale, J.D.; Warren, M.C. Rigid unit modes and the negative thermal expansion in $ZrW_2O_8$. *Phase Transit.* **1997**, *61*, 141–153.
38. Stillinger, F.H.; Stillinger, D.K. Negative thermal expansion in the Gaussian core model. *Phys. A* **1997**, *244*, 358–369.
39. David, W.I.F.; Evans, J.S.O.; Sleight, A.W. Direct evidence for a low-frequency phonon mode mechanism in the negative thermal expansion compound $ZrW_2O_8$. *Europhys. Lett.* **1999**, *46*, 661–666.
40. Heine, V.; Welche, P.R.L.; Dove, M.T. Geometrical origin and theory of negative thermal expansion in framework structures. *J. Am. Ceram. Soc.* **1999**, *82*, 1793–1802.
41. Ramirez, A.P.; Broholm, C.L.; Cava, R.J.; Kowach, G.R. Geometrical frustration, spin ice and negative thermal expansion—The physics of underconstraint. *Phys. B Condens. Matter* **2000**, *280*, 290–295.
42. Boerio-Goates, J.; Stevens, R.; Lang, B.; Woodfield, B.F. Heat capacity calorimetry—Detection of low frequency modes in solids and an application to negative thermal expansion materials. *J. Therm. Anal. Calorim.* **2002**, *69*, 773–783.
43. Chapman, K.W.; Chupas, P.J. Anomalous thermal expansion of cuprites: A combined high resolution pair distribution function and geometric analysis. *Chem. Mater.* **2009**, *21*, 425–431.

44. Korcok, J.L.; Katz, M.J.; Leznoff, D.B. Impact of metallophilicity on "colossal" positive and negative thermal expansion in a series of isostructural dicyanometallate coordination polymers. *J. Am. Chem. Soc.* **2009**, *131*, 4866–4871.
45. Sleight, A.W.; Thundathil, M.A.; Evans, J.S.O. Negative Thermal Expansion Materials. *U.S. Patent 5,514,360*, 7 May 1996.
46. Sleight, A.W. Compounds that contract on heating. *Inorg. Chem.* **1998**, *37*, 2854–2860.
47. Sleight, A.W. Isotropic negative thermal expansion. *Ann. Rev. Mater. Sci.* **1998**, *28*, 29–43.
48. Fleming, D.A.; Johnson, D.W.; Lemaire, P.J. Article Comprising a Temperature Compensated Optical Fiber Refractive Index Grating. *U.S. Patent 5,694,503*, 2 December 1997.
49. Verdon, C.; Dunand, D.C. High-temperature reactivity in the $ZrW_2O_8$-Cu system. *Scr. Mater.* **1997**, *36*, 1075–1080.
50. Balch, D.K.; Dunand, D.C. Copper-zirconium tungstate composites exhibiting low and negative thermal expansion influenced by reinforcement phase transformations. *Metall. Mater. Trans. A* **2004**, *35*, 1159–1165.
51. De Buysser, K.; Lommens, P.; de Meyer, C.; Bruneel, E.; Hoste, S.; van Driessche, I. $ZrO_2$-$ZrW_2O_8$ composites with tailor-made thermal expansion. *Ceram. Silik.* **2004**, *48*, 139–144.
52. Lommens, P.; de Meyer, C.; Bruneel, E.; de Buysser, K.; van Driessche, I.; Hoste, S. Synthesis and thermal expansion of $ZrO_2/ZrW_2O_8$ composites. *J. Eur. Ceram. Soc.* **2005**, *25*, 3605–3610.
53. Evans, J.S.O.; Mary, T.A.; Vogt, T.; Subramanian, M.A.; Sleight, A.W. Negative thermal expansion in $ZrW_2O_8$ and $HfW_2O_8$. *Chem. Mater.* **1996**, *8*, 2809–2823.
54. Lind, C.; Wilkinson, A.P.; Hu, Z.B.; Short, S.; Jorgensen, J.D. Synthesis and properties of the negative thermal expansion material cubic $ZrMo_2O_8$. *Chem. Mater.* **1998**, *10*, 2335–2337.
55. Attfield, M.P.; Sleight, A.W. Exceptional negative thermal expansion in $AlPO_4$-17. *Chem. Mater.* **1998**, *10*, 2013–2019.
56. Attfield, M.P.; Sleight, A.W. Strong negative thermal expansion in siliceous faujasite. *Chem. Commun.* **1998**, 601–602.
57. Goodwin, A.L.; Chapman, K.W.; Kepert, C.J. Guest-dependent negative thermal expansion in nanoporous Prussian Blue analogues $M^{II}Pt^{IV}(CN)_6$ $\{H_2O\}$ $(0 \leq x \leq 2$; M = Zn, Cd). *J. Am. Chem. Soc.* **2005**, *127*, 17980–17981.
58. Margadonna, S.; Prassides, K.; Fitch, A.N. Zero thermal expansion in a Prussian blue analogue. *J. Am. Chem. Soc.* **2004**, *126*, 15390–15391.
59. Tao, J.Z.; Sleight, A.W. The role of rigid unit modes in negative thermal expansion. *J. Solid State Chem.* **2003**, *173*, 442–448.
60. Bieniok, A.; Hammonds, K.D. Rigid unit modes and the phase transition and structural distortions of zeolite rho. *Microporous Mesoporous Mat.* **1998**, *25*, 193–200.
61. Dove, M.T.; Hammonds, K.D.; Harris, M.J.; Heine, V.; Keen, D.A.; Pryde, A.K.A.; Trachenko, K.; Warren, M.C. Amorphous silica from the Rigid unit mode approach. *Miner. Mag.* **2000**, *64*, 377–388.
62. Dove, M.T.; Trachenko, K.O.; Tucker, M.G.; Keen, D.A. Rigid unit modes in framework structures: Theory, experiment and applications. *Rev. Mineral. Geochem.* **2000**, *39*, 1–33.

63. Yamamura, Y.; Nakajima, N.; Tsuji, T.; Iwasa, Y.; Saito, K.; Sorai, M. Heat capacity and Gruneisen functions of negative thermal expansion compound $HfW_2O_8$. *Solid State Commun.* **2002**, *121*, 213–217.
64. Mittal, R.; Chaplot, S.L. Phonon density of states and thermodynamic properties in cubic and orthorhombic phases of $ZrW_2O_8$. *Solid State Commun.* **2000**, *115*, 319–322.
65. Mittal, R.; Chaplot, S.L.; Schober, H.; Kolesnikov, A.I.; Loong, C.K.; Lind, C.; Wilkinson, A.P. Negative thermal expansion in cubic $ZrMo_2O_8$: Inelastic neutron scattering and lattice dynamical studies. *Phys. Rev. B* **2004**, *70*, 214303:1–214303:6.
66. Auray, M.; Quarton, M. Zirconium tungstate. *Acta Crystallogr. C* **1995**, *51*, 2210–2213.
67. Closmann, C.; Sleight, A.W.; Haygarth, J.C. Low-temperature synthesis of $ZrW_2O_8$ and Mo-substituted $ZrW_2O_8$. *J. Solid State Chem.* **1998**, *139*, 424–426.
68. Allen, S.; Evans, J.S.O. Negative thermal expansion and oxygen disorder in cubic $ZrMo_2O_8$. *Phys. Rev. B* **2003**, *68*, 134101:1–134101:3.
69. Lind, C.; Wilkinson, A.P.; Rawn, C.J.; Payzant, E.A. Preparation of the negative thermal expansion material cubic $ZrMo_2O_8$. *J. Mater. Chem.* **2001**, *11*, 3354–3359.
70. Lind, C.; Wilkinson, A.P.; Rawn, C.J.; Payzant, E.A. Kinetics of the cubic to trigonal transformation in $ZrMo_2O_8$ and their dependence on precursor chemistry. *J. Mater. Chem.* **2002**, *12*, 990–994.
71. Readman, J.E.; Lister, S.E.; Peters, L.; Wright, J.; Evans, J.S.O. Direct synthesis of cubic $ZrMo_2O_8$ followed by ultrafast in situ powder diffraction. *J. Amer. Chem. Soc.* **2009**, *131*, 17560–17562.
72. Evans, J.S.O.; Hanson, P.A.; Ibberson, R.M.; Duan, N.; Kameswari, U.; Sleight, A.W. Low-temperature oxygen migration and negative thermal expansion in $ZrW_{2-x}Mo_xO_8$. *J. Am. Chem. Soc.* **2000**, *122*, 8694–8699.
73. Kameswari, U.; Sleight, A.W.; Evans, J.S.O. Rapid synthesis of $ZrW_2O_8$ and related phases, and structure refinement of $ZrWMoO_8$. *Int. J. Inorg. Mater.* **2000**, *2*, 333–337.
74. Allen, S.; Evans, J.S.O. The kinetics of low-temperature oxygen migration in $ZrWMoO_8$. *J. Mater. Chem.* **2004**, *14*, 151–156.
75. De Meyer, C.; Bouree, F.; Evans, J.S.O.; de Buysser, K.; Bruneel, E.; van Driessche, I.; Hoste, S. Structure and phase transition of Sn-substituted $Zr_{1-x}Sn_xW_2O_8$. *J. Mater. Chem.* **2004**, *14*, 2988–2994.
76. De Buysser, K.; van Driessche, I.; Putte, B.V.; Vanhee, P.; Schaubroeck, J.; Hoste, S. Study of negative thermal expansion and shift in phase transition temperature in $Ti^{4+}$- and $Sn^{4+}$-substituted ZrW2O8 materials. *Inorg. Chem.* **2008**, *47*, 736–741.
77. Nakajima, N.; Yamamura, Y.; Tsuji, T. Synthesis and physical properties of negative thermal expansion materials $Zr_{1-x}M_xW_2O_{8-y}$ (M = Sc, In, Y) substituted for Zr(IV) sites by M(III) ions. *Solid State Commun.* **2003**, *128*, 193–196.
78. Hashimoto, T.; Kuwahara, J.; Yoshida, T.; Nashimoto, M.; Takahashi, Y.; Takahashi, K.; Morito, Y. Thermal conductivity of negative-thermal-expansion oxide, $Zr_{1-x}Y_xW_2O_8$ (x = 0.00, 0.01): Temperature dependence and effect of structural phase transition. *Solid State Commun.* **2004**, *131*, 217–221.

79. Tsuji, T.; Yamamura, Y.; Nakajima, N. Thermodynamic properties of negative thermal expansion materials $ZrW_2O_8$ substituted for Zr site. *Thermochim. Acta* **2004**, *416*, 93–98.
80. Yamamura, Y.; Nakajima, N.; Tsuji, T.; Kojima, A.; Kuroiwa, Y.; Sawada, A.; Aoyagi, S.; Kasatani, H. Drastic lowering of the order-disorder phase transition temperatures in $Zr_{1-x}M_xW_2O_{8-y}$ (M = Sc,Y,In) solidsolutions. *Phys. Rev. B* **2004**, *70*, 104107:1–104107:6.
81. Yamamura, Y.; Masago, K.; Kato, M.; Tsuji, T. Comprehensive interpretation of a substitution effect on an order-disorder phase transition in $A_{1-x}M_xW_2O_{8-y}$ (A = Zr, Hf; M = trivalent cations) and other $ZrW_2O_8$-based solid solutions. *J. Phys. Chem. B* **2007**, *111*, 10118–10122.
82. Chen, X.; Tao, J.; Ma, H.; Zhao, X. Disordered structure of $ZrW_{1.8}V_{0.2}O_{7.9}$ from a combined X-ray and neutron powder diffraction study at 530 K. *Acta Crystallogr. C* **2009**, *65*, 74–76.
83. Chen, X.; Deng, X.; Ma, H.; Tao, J.; Zhao, X. Hydrothermal synthesis and thermal properties of a novel cubic $ZrW_{1.80}V_{0.20}O_{7.90}$ solid solution. *J. Solid State Chem.* **2011**, *184*, 1090–1095.
84. Hu, Z.; Jorgensen, J.D.; Teslic, S.; Short, S.; Argyriou, D.N.; Evans, J.S.O.; Sleight, A.W. Pressure-induced phase transformation in $ZrW_2O_8$: Compressibility and thermal expansion of the orthorhombic phase. *Physica B* **1997**, *241*, 370–372.
85. Jorgensen, J.D.; Hu, Z.; Teslic, S.; Argyriou, D.N.; Short, S.; Evans, J.S.O.; Sleight, A.W. Pressure-induced cubic-to-orthorhombic phase transition in $ZrW_2O_8$. *Phys. Rev. B* **1999**, *59*, 215–225.
86. Grzechnik, A.; Crichton, W.A.; Syassen, K.; Adler, P.; Mezouar, M. A new polymorph of $ZrW_2O_8$ synthesized at high pressures and high temperatures. *Chem. Mater.* **2001**, *13*, 4255–4259.
87. Keen, D.A.; Goodwin, A.L.; Tucker, M.G.; Dove, M.T.; Evans, J.S.O.; Crichton, W.A.; Brunelli, M. Structural description of pressure-induced amorphization in $ZrW_2O_8$. *Phys. Rev. Lett.* **2007**, *98*, 225501:1–225501:4.
88. Chen, B.; Muthu, D.V.S.; Liu, Z.X.; Sleight, A.W.; Kruger, M.B. High-pressure optical study of $HfW_2O_8$. *J. Phys. Condens. Matter* **2002**, *14*, 13911–13916.
89. Jorgensen, J.D.; Hu, Z.; Short, S.; Sleight, A.W.; Evans, J.S.O. Pressure-induced cubic-to-orthorhombic phase transformation in the negative thermal expansion material $HfW_2O_8$. *J. Appl. Phys.* **2001**, *89*, 3184–3188.
90. Lind, C.; VanDerveer, D.G.; Wilkinson, A.P.; Chen, J.H.; Vaughan, M.T.; Weidner, D.J. New high-pressure form of the negative thermal expansion materials zirconium molybdate and hafnium molybdate. *Chem. Mater.* **2001**, *13*, 487–490.
91. Grzechnik, A.; Crichton, W.A. Structural transformations in cubic $ZrMo_2O_8$ at high pressures and high temperatures. *Solid State Sci.* **2002** ,*4*, 1137–1141.
92. Varga, T.; Wilkinson, A.P.; Lind, C.; Bassett, W.A.; Zha, C.S. Pressure-induced amorphization of cubic $ZrMo_2O_8$ studied in situ by X-ray absorption spectroscopy and diffraction. *Solid State Commun.* **2005**, *135*, 739–744.
93. Evans, J.S.O.; Jorgensen, J.D.; Short, S.; David, W.I.F.; Ibberson, R.M.; Sleight, A.W. Thermal expansion in the orthorhombic gamma phase of $ZrW_2O_8$. *Phys. Rev. B* **1999**, *60*, 14643–14648.
94. Varga, T.; Wilkinson, A.P.; Jupe, A.C.; Lind, C.; Bassett, W.A.; Zha, C.S. Pressure-induced amorphization of cubic $ZrW_2O_8$ studied in situ and ex situ by synchrotron X-ray diffraction and absorption. *Phys. Rev. B* **2005**, *72*, 024117:1–024117:10.

95. Evans, J.S.O.; Hanson, J.C.; Sleight, A.W. Room-temperature superstructure of $ZrV_2O_7$. *Acta Crystallogr. B* **1998**, *54*, 705–713.
96. Khosrovani, K.; Sleight, A.W.; Vogt, T. Structure of $ZrV_2O_7$ from −263 to 470 degrees C. *J. Solid State Chem.* **1997**, *132*, 355–360.
97. Withers, R.L.; Evans, J.S.O.; Hanson, J.C.; Sleight, A.W. An in-situ tempertaure dependent electron and X-ray diffraction study of the structural phase transitions in $ZrV_2O_7$. *J. Solid State Chem.* **1998**, *137*, 161–167.
98. Onken, H. Ueber zirkonpyroarsenat. *Naturwissenschaften* **1965**, *52*, 344.
99. Le Flem, G.; Lamic, J.; Hagenmuller, P. $As_2O_5$-$ThO_2$ system. *Bull. Soc. Chim. Fr.* **1966**, *6*, 1880–1883.
100. Losilla, E.R.; Cabeza, A.; Bruque, S.; Aranda, M.A.G.; Sanz, J.; Iglesias, J.E.; Alonso, J.A. Syntheses, structures, and thermal expansion of germanium pyrophosphates. *J. Solid State Chem.* **2001**, *156*, 213–219.
101. Fayon, F.; King, I.J.; Harris, R.K.; Gover, R.K.B.; Evans, J.S.O.; Massiot, D. Characterization of the room-temperature structure of $SnP_2O_7$ by $P^{31}$ through-space and through-bond NMR correlation spectroscopy. *Chem. Mater.* **2003**, *15*, 2234–2239.
102. Gover, R.K.B.; Withers, N.D.; Allen, S.; Withers, R.L.; Evans, J.S.O. Structure and phase transitions of $SnP_2O_7$. *J. Solid State Chem.* **2002**, *166*, 42–48.
103. White, K.M.; Lee, P.L.; Chupas, P.J.; Chapman, K.W.; Payzant, E.A.; Jupe, A.C.; Bassett, W.A.; Zha, C.S.; Wilkinson, A.P. Synthesis, symmetry, and physical properties of cerium pyrophosphate. *Chem. Mater.* **2008**, *20*, 3728–3734.
104. Wallez, G.; Raison, P.E.; Dacheux, N.; Clavier, N.; Bykov, D.; Delevoye, L.; Popa, K.; Bregiroux, D.; Fitch, A.N.; Konings, R.J.M. Triclinic-cubic phase transition and negative expansion in the actinide IV (Th, U, Np, Pu) diphosphates. *Inorg. Chem.* **2012**, *51*, 4314–4322.
105. Stinton, G.W.; Hampson, M.R.; Evans, J.S.O. The 136-atom structure of $ZrP_2O_7$ and $HfP_2O_7$ from powder diffraction data. *Inorg. Chem.* **2006**, *45*, 4352–4358.
106. Birkedal, H.; Andersen, A.M.K.; Arakcheeva, A.; Chapuis, G.; Norby, P.; Pattison, P. The room-temperature superstructure of $ZrP_2O_7$ is orthorhombic: There are no unusual 180° P-O-P bond angles. *Inorg. Chem.* **2006**, *45*, 4346–4351.
107. Oyetola, S.; Verbaere, A.; Guyomard, D.; Crosnier, M.P.; Piffard, Y.; Tournoux, M. New $ZrP_2O_7$-like diphosphates of either mixed ($M_{1/2}$(III)$M'_{1/2}$(V)) cations (M = Sb, Bi, Nd, Eu-M' = Sb, Nb, Ta) or M'V cations (M' = Ta, Nb)—Synthesis and structure. *Eur. J. Solid State Inorg. Chem.* **1991**, *28*, 23–36.
108. Varga, T.; Wilkinson, A.P.; Haluska, M.S.; Payzant, E.A. Preparation and thermal expansion of $(M^{III}0.5M'^{V}0.5)P_2O_7$ with the cubic $ZrP_2O_7$ structure. *J. Solid State Chem.* **2005**, *178*, 3541–3546.
109. Yanase, I.; Kojima, T.; Kobayashi, H. Effects of Nb and Y substitution on negative thermal expansion of $ZrV_{2-x}P_xO_7$ ($0 \leq X \leq 0.8$). *Solid State Commun.* **2011**, *151*, 595–598.
110. Sahoo, P.P.; Sumithra, S.; Madras, G.; Row, T.N.G. Synthesis, structure, negative thermal expansion, and photocatalytic property of Mo doped $ZrV_2O_7$. *Inorg. Chem.* **2011**, *50*, 8774–8781.
111. Carlson, S.; Andersen, A.M.K. High-pressure properties of $TiP_2O_7$, $ZrP_2O_7$ and $ZrV_2O_7$. *J. Appl. Crystallogr.* **2001**, *34*, 7–12.

112. Hemamala, U.L.C.; El-Ghussein, F.; Muthu, D.V.S.; Andersen, A.M.K.; Carlson, S.; Ouyang, L.; Kruger, M.B. High-pressure Raman and infrared study of $ZrV_2O_7$. *Solid State Commun.* **2007**, *141*, 680–684.
113. Lipinska-Kalita, K.E.; Kruger, M.B.; Carlson, S.; Andersen, A.M.K. High-pressure studies of titanium pyrophosphate by Raman scattering and infrared spectroscopy. *Physica B* **2003**, *337*, 221–229.
114. Petruska, E.A.; Muthu, D.V.S.; Carlson, S.; Andersen, A.M.K.; Ouyang, L.; Kruger, M.B. High-pressure Raman and infrared spectroscopic studies of $ZrP_2O_7$. *Solid State Commun.* **2010**, *150*, 235–239.
115. Evans, J.S.O.; Mary, T.A.; Sleight, A.W. Negative thermal expansion in $Sc_2(WO_4)_3$. *J. Solid State Chem.* **1998**, *137*, 148–160.
116. Zhou, Y.; Adams, S.; Rao, R.P.; Edwards, D.D.; Neiman, A.; Pestereva, N. Charge transport by polyatomic anion diffusion in $Sc_2(WO_4)_3$. *Chem. Mater.* **2008**, *20*, 6335–6345.
117. Evans, J.S.O.; Mary, T.A. Structural phase transitions and negative thermal expansion in $Sc_2(MoO_4)_3$. *Int. J. Inorg. Mater.* **2000**, *2*, 143–151.
118. Wu, M.M.; Cheng, Y.Z.; Peng, J.; Xiao, X.L.; Chen, D.F.; Kiyanagi, R.; Fieramosca, J.S.; Short, S.; Jorgensen, J.; Hu, Z.B. Synthesis of solid solution $Er_{2-x}Ce_xW_3O_{12}$ and studies of their thermal expansion behavior. *Mater. Res. Bull.* **2007**, *42*, 2090–2098.
119. Wu, M.M.; Peng, J.; Cheng, Y.Z.; Xiao, X.L.; Hao, Y.M.; Hu, Z.B. Thermal expansion in solid solution $Er_{2-x}Sm_xW_3O_{12}$. *Mater. Sci. Eng. B* **2007**, *137*, 144–148.
120. Wu, M.M.; Peng, J.; Cheng, Y.Z.; Wang, H.; Yu, Z.X.; Chen, D.F.; Hu, Z.B. Structure and thermal expansion properties of solid solution $Nd_{2-x}Er_xW_3O_{12}$ ($0.0 \leq x \leq 0.6$ and $1.5 \leq x \leq 2.0$). *Solid State Sci.* **2006**, *8*, 665–670.
121. Xiao, X.L.; Peng, J.; Wu, M.M.; Cheng, Y.Z.; Chen, D.F.; Hu, Z.B. The crystal structure and thermal expansion properties of solid solutions $Ln_{2-x}Dy_xW_3O_{12}$ (Ln = Er and Y). *J. Alloy. Compd.* **2008**, *465*, 556–561.
122. Peng, J.; Wu, M.M.; Wang, H.; Hao, Y.M.; Hu, Z.; Yu, Z.X.; Chen, D.F.; Kiyanagic, R.; Fieramosca, J.S.; Short, S.; Jorgensen, J. Structures and negative thermal expansion properties of solid solutions $Y_xNd_{2-x}W_3O_{12}$ (x = 0.0–1.0, 1.6–2.0). *J. Alloy. Compd.* **2008**, *453*, 49–54.
123. Evans, J.S.O.; Mary, T.A.; Sleight, A.W. Structure of $Zr_2(WO_4)(PO_4)_2$ from powder X-ray data: Cation ordering with no superstructure. *J. Solid State Chem.* **1995**, *120*, 101–104.
124. Cetinkol, M.; Wilkinson, A.P.; Lee, P.L. Structural changes accompanying negative thermal expansion in $Zr_2(MoO_4)(PO_4)_2$. *J. Solid State Chem.* **2009**, *182*, 1304–1311.
125. Suzuki, T.; Omote, A. Negative thermal expansion in $(HfMg)(WO_4)_3$. *J. Am. Ceram. Soc.* **2004**, *87*, 1365–1367.
126. Gindhart, A.M.; Lind, C.; Green, M. Polymorphism in the negative thermal expansion material magnesium hafnium tungstate. *J. Mater. Res.* **2008**, *23*, 210–213.
127. Marinkovic, B.A.; Jardim, P.M.; Ari, M.; de Avillez, R.R.; Rizzo, F.; Ferreira, F.F. Low positive thermal expansion in $HfMgMo_3O_{12}$. *Phys. Status Solidi B* **2008**, *245*, 2514–2519.
128. Sleight, A.W.; Brixner, L.H. A New Ferroelastic transition in some $A_2(MO_4)_3$ molybdates and tungstates. *J. Solid State Chem.* **1973**, *7*, 172–174.

129. Forster, P.M.; Sleight, A.W. Negative thermal expansion in $Y_2W_3O_{12}$. *Int. J. Inorg. Mater.* **1999**, *1*, 123–127.
130. Suzuki, T.; Omote, A. Zero thermal expansion in $(Al_{2x}(HfMg)_{1-x})(WO_4)_3$. *J. Am. Ceram. Soc.* **2006**, *89*, 691–693.
131. Marinkovic, B.A.; Jardim, P.M.; de Avillez, R.R.; Rizzo, F. Negative thermal expansion in $Y_2Mo_3O_{12}$. *Solid State Sci.* **2005**, *7*, 1377–1383.
132. Sumithra, S.; Tyagi, A.K.; Umarji, A.M. Negative thermal expansion in $Er_2W_3O_{12}$ and $Yb_2W_3O_{12}$ by high temperature X-ray diffraction. *Mater. Sci. Eng. B* **2005**, *116*, 14–18.
133. Gates, S.D.; Lind, C. Polymorphism in yttrium molybdate $Y_2Mo_3O_{12}$. *J. Solid State Chem.* **2007**, *180*, 3510–3514.
134. Varga, T.; Wilkinson, A.P.; Jorgensen, J.D.; Short, S. Neutron powder diffraction study of the orthorhombic to monoclinic transition in $Sc_2W_3O_{12}$ on compression. *Solid State Sci.* **2006**, *8*, 289–295.
135. Varga, T.; Wilkinson, A.P.; Lind, C.; Bassett, W.A.; Zha, C.S. High pressure synchrotron X-ray powder diffraction study of $Sc_2Mo_3O_{12}$ and $Al_2W_3O_{12}$. *J. Phys. Condens. Matter* **2005**, *17*, 4271–4283.
136. Varga, T.; Wilkinson, A.P.; Lind, C.; Bassett, W.A.; Zha, C.S. In situ high-pressure synchrotron X-ray diffraction study of $Sc_2W_3O_{12}$ at up to 10 GPa. *Phys. Rev. B* **2005**, *71*, 214106:1–214106:8.
137. Garg, N.; Murli, C.; Tyagi, A.K.; Sharma, S.M. Phase transitions in $Sc_2(WO_4)_3$ under high pressure. *Phys. Rev. B* **2005**, *72*, 064106:1–064106:7.
138. Garg, N.; Panchal, V.; Tyagi, A.K.; Sharma, S.M. Pressure-induced phase transitions in $Al_2(WO_4)_3$. *J. Solid State Chem.* **2005**, *178*, 998–1002.
139. Achary, S.N.; Mukherjee, G.D.; Tyagi, A.K.; Vaidya, S.N. Preparation, thermal expansion, high pressure and high temperature behavior of $Al_2(WO_4)_3$. *J. Mater. Sci.* **2002**, *37*, 2501–2509.
140. Arora, A.K.; Nithya, R.; Yagi, T.; Miyajima, N.; Mary, T.A. Two-stage amorphization of scandium molybdate at high pressure. *Solid State Commun.* **2004**, *129*, 9–13.
141. Baiz, T.I.; Heinrich, C.P.; Banek, N.A.; Vivekens, B.L.; Lind, C. In-situ non-ambient X-ray diffraction studies of indium tungstate. *J. Solid State Chem.* **2012**, *187*, 195–199.
142. Liu, H.; Secco, R.A.; Imanaka, N.; Rutter, M.D.; Adachi, G.; Uchida, T. Ionic to electronic dominant conductivity in $Al_2(WO_4)_3$ at high pressure and high temperature. *J. Phys. Chem. Solids* **2003**, *64*, 287–294.
143. Mukherjee, G.D.; Vijaykumar, V.; Achary, S.N.; Tyagi, A.K.; Godwal, B.K. Phase transitions in $Al_2(WO_4)_3$: High pressure investigations of low frequency dielectric constant and crystal structure. *J. Phys. Condens. Matter* **2004**, *16*, 7321–7330.
144. Secco, R.A.; Liu, H.; Imanaka, N.; Adachi, G.; Rutter, M.D. Electrical conductivity and amorphization Of $Sc_2(WO_4)_3$ at high pressures and temperatures. *J. Phys. Chem. Solids* **2002**, *63*, 425–431.
145. Cetinkol, M.; Wilkinson, A.P.; Lind, C. In situ high-pressure synchrotron X-ray diffraction study of $Zr_2(WO_4)(PO_4)_2$ up to 16 GPa. *Phys. Rev. B* **2009**, *79*, 224118:1–224118:10.
146. Gates, S.D.; Colin, J.A.; Lind, C. Non-hydrolytic sol-gel synthesis, properties, and high-pressure behavior of gallium molybdate. *J. Mater. Chem.* **2006**, *16*, 4214–4219.

147. Karmakar, S.; Deb, S.K.; Tyagi, A.K.; Sharma, S.M. Pressure-induced amorphization in $Y_2(WO_4)_3$: In situ X-ray diffraction and Raman studies. *J. Solid State Chem.* **2004**, *177*, 4087–4092.
148. Miller, W.; Smith, C.W.; Mackenzie, D.S.; Evans, K.E. Negative thermal expansion: A review. *J. Mater. Sci.* **2009**, *44*, 5441–5451.
149. Woodcock, D.A.; Lightfoot, P.; Villaescusa, L.A.; Diaz-Cabanas, M.J.; Camblor, M.A.; Engberg, D. Negative thermal expansion in the siliceous zeolites chabazite and ITQ-4: A neutron powder diffraction study. *Chem. Mater.* **1999**, *11*, 2508–2514.
150. Taylor, D. Thermal expansion data V. Miscellaneous binary oxides. *Trans. J. Br. Ceram. Soc.* **1985**, *84*, 9–14.
151. Sanson, A.; Rocca, F.; Dalba, G.; Fornasini, P.; Grisenti, R.; Dapiaggi, M.; Artioli, G. Negative thermal expansion and local dynamics in $Cu_2O$ and $Ag_2O$. *Phys. Rev. B* **2006**, *73*, 214305:1–214305:13.
152. Li, J.; Yokochi, A.; Amos, T.G.; Sleight, A.W. Strong negative thermal expansion along the O-Cu-O linkage in $CuScO_2$. *Chem. Mater.* **2002**, *14*, 2602–2606.
153. Li, J.; Sleight, A.W.; Jones, C.Y.; Toby, B.H. Trends in negative thermal expansion behavior for $AMO_2$ (A = Cu or Ag; M = Al, Sc, In, or La) compounds with the delafossite structure. *J. Solid State Chem.* **2005**, *178*, 285–294.
154. Ahmed, S.I.; Dalba, G.; Fornasini, P.; Vaccari, M.; Rocca, F.; Sanson, A.; Li, J.; Sleight, A.W. Negative thermal expansion in crystals with the delafossite structure: An extended X-ray absorption fine structure study of $CuScO_2$ and $CuLaO_2$. *Phys. Rev. B* **2009**, *79*, 104302:1–104302:8.
155. Barreteau, C.; Bregiroux, D.; Laurent, G.; Wallez, G. Reducing ultra-low thermal expansion of beta-$Zr_2O(PO_4)_2$ by substitutions? *Mater. Res. Bull.* **2010**, *45*, 1996–2000.
156. Clavier, N.; Wallez, G.; Dacheux, N.; Bregiroux, D.; Quarton, M.; Beaunier, P. Synthesis, Raman and Rietveld analysis of thorium diphosphate. *J. Solid State Chem.* **2008**, *181*, 3352–3356.
157. Wallez, G.; Bregiroux, D.; Quarton, M. Mechanism of the low thermal expansion in α-$Hf_2O(PO_4)_2$ and its zirconium analog. *J. Solid State Chem.* **2008**, *181*, 1413–1418.
158. Wallez, G.; Clavier, N.; Dacheux, N.; Bregiroux, D. Negative thermal expansion in $Th_2O(PO_4)_2$. *Mater. Res. Bull.* **2011**, *46*, 1777–1780.
159. Wallez, G.; Launay, S.; Quarton, M.; Dacheux, N.; Soubeyroux, J.L. Why does uranium oxide phosphate contract on heating? *J. Solid State Chem.* **2004**, *177*, 3575–3580.
160. Dapiaggi, M.; Fitch, A.N. Negative (and very low) thermal expansion in $ReO_3$ from 5 to 300 K. *J. Appl. Crystallogr.* **2009**, *42*, 253–258.
161. Amos, T.G.; Sleight, A.W. Negative thermal expansion in orthorhombic $NbOPO_4$. *J. Solid State Chem.* **2001**, *160*, 230–238.
162. Amos, T.G.; Yokochi, A.; Sleight, A.W. Phase transition and negative thermal expansion in tetragonal $NbOPO_4$. *J. Solid State Chem.* **1998**, *141*, 303–307.
163. Mukherjee, G.D.; Vijaykumar, V.; Karandikar, A.S.; Godwal, B.K.; Achary, S.N.; Tyagi, A.K.; Lausi, A.; Busetto, E. Compressibility anomaly and amorphization in the anisotropic negative thermal expansion material $NbOPO_4$ under pressure. *J. Solid State Chem.* **2005**, *178*, 8–14.
164. Wang, J.; Deng, J.; Yu, R.; Chen, J.; Xing, X. Coprecipitation synthesis and negative thermal expansion of $NbVO_5$. *Dalton Trans.* **2011**, *40*, 3394–3397.

165. Wang, X.; Huang, Q.; Deng, J.; Yu, R.; Chen, J.; Xing, X. Phase transformation and negative thermal expansion in $TaVO_5$. *Inorg. Chem.* **2011**, *50*, 2685–2690.
166. Greve, B.K.; Martin, K.L.; Lee, P.L.; Chupas, P.J.; Chapman, K.W.; Wilkinson, A.P. Pronounced negative thermal expansion from a simple structure: Cubic $ScF_3$. *J. Am. Chem. Soc.* **2010**, *132*, 15496–15498.
167. Williams, D.J.; Partin, D.E.; Lincoln, F.J.; Kouvetakis, J.; O'Keeffe, M. The disordered crystal structures of $Zn(CN)_2$ and $Ga(CN)_3$. *J. Solid State Chem.* **1997**, *134*, 164–169.
168. Goodwin, A.L.; Kepert, C.J. Negative thermal expansion and low-frequency modes in cyanide-bridged framework materials. *Phys. Rev. B* **2005**, *71*, 140301:1–140301:4.
169. Adak, S.; Daemen, L.L.; Hartl, M.; Williams, D.; Summerhill, J.; Nakotte, H. Thermal expansion in 3d-metal Prussian blue analogs—A survey study. *J. Solid State Chem.* **2011**, *184*, 2854–2861.
170. Goodwin, A.L.; Kennedy, B.J.; Kepert, C.J. Thermal expansion matching via framework flexibility in Zinc dicyanometallates. *J. Am. Chem. Soc.* **2009**, *131*, 6334–6335.
171. Conterio, M.J.; Goodwin, A.L.; Tucker, M.G.; Keen, D.A.; Dove, M.T.; Peters, L.; Evans, J.S.O. Local structure in $Ag_3[Co(CN)_6]$: Colossal thermal expansion, rigid unit modes and argentophilic interactions. *J. Phys. Condens. Matter* **2008**, *20*, doi:10.1088/0953-8984/20/25/255225.
172. Goodwin, A.L.; Keen, D.A.; Tucker, M.G.; Dove, M.T.; Peters, L.; Evans, J.S.O. Argentophilicity-dependent colossal thermal expansion in extended Prussian blue analogues. *J. Am. Chem. Soc.* **2008**, *130*, 9660–9661.
173. Kozy, L.C.; Tahir, M.N.; Lind, C.; Tremel, W. Particle size and morphology control of the negative thermal expansion material cubic zirconium tungstate. *J. Mater. Chem.* **2009**, *19*, 2760–2765.
174. Nikolov, V.; Koseva, I.; Stoyanova, R.; Zhecheva, E. Conditions for preparation of nanosized $Al_2(WO_4)_3$. *J. Alloy. Compd.* **2010**, *505*, 443–449.
175. Duan, N.; Kameswari, U.; Sleight, A.W. Further contraction of $ZrW_2O_8$. *J. Am. Chem. Soc.* **1999**, *121*, 10432–10433.
176. Lind, C. Negative Thermal Expansion Materials Related to Cubic Zirconium Tungstate. Ph.D. Dissertation, Georgia Institute of Technology, Atlanta, GA, USA, 2001.
177. Banek, N.A.; Baiz, H.I.; Latigo, A.; Lind, C. Autohydration of nanosized cubic zirconium tungstate. *J. Amer. Chem. Soc.* **2010**, *132*, 8278–8279.
178. Sullivan, L.M.; Lukehart, C.M. Zirconium tungstate ($ZrW_2O_8$)/polyimide nanocomposites exhibiting reduced coefficient of thermal expansion. *Chem. Mater.* **2005**, *17*, 2136–2141.
179. Sharma, G.R.; Coleman, M.R.; Lind, C. Polyimide nanocomposites for tunable coefficient of thermal expansion. In *Proceedings of the 40th International SAMPE Technical Conference* Memphis, TN, USA, 8–11 September 2008.
180. Lind, C.; Coleman, M.R.; Kozy, L.C.; Sharma, G.R. Zirconium tungstate/polymer nanocomposites: Challenges and opportunities. *Phys. Status Solidi B* **2011**, *248*, 123–129.
181. Cho, C.H.; Oh, K.Y.; Kim, S.K.; Yeo, J.G.; Lee, Y.M. Improvement in thermal stability of NaA zeolite composite membrane by control of intermediate layer structure. *J. Membr. Sci.* **2011**, *366*, 229–236.

182. Cho, C.H.; Oh, K.Y.; Yeo, J.G.; Kim, S.K.; Lee, Y.M. Synthesis, ethanol dehydration and thermal stability of NaA zeolite/alumina composite membranes with narrow non-zeolitic pores and thin intermediate layer. *J. Membr. Sci.* **2010**, *364*, 138–148.
183. Akhtar, F.; Ojuva, A.; Wirawan, S.K.; Hedlund, J.; Bergstrom, L. Hierarchically porous binder-free silicalite-1 discs: A novel support for all-zeolite membranes. *J. Mater. Chem.* **2011**, *21*, 8822–8828.
184. Tran, K.D.; Groshens, T.J.; Nelson, J.G. Fabrication of near-zero thermal expansion $(Fe_xSc_{1-x})_2Mo_3O_{12}$-$MoO_3$ ceramic composite using the reaction sintering process. *Mater. Sci. Eng. A* **2001**, *303*, 234–240.
185. Watanabe, H.; Tani, J.; Kido, H.; Mizuuchi, K. Thermal expansion and mechanical properties of pure magnesium containing zirconium tungsten phosphate particles with negative thermal expansion. *Mater. Sci. Eng. A* **2008**, *494*, 291–298.
186. Holzer, H.; Dunand, D.C. Phase transformation and thermal expansion of Cu/$ZrW_2O_8$ metal matrix composites. *J. Mater. Res.* **1999**, *14*, 780–789.
187. Yilmaz, S.; Dunand, D.C. Finite-element analysis of thermal expansion and thermal mismatch stresses in a Cu-60vol%$ZrW_2O_8$ composite. *Compos. Sci. Technol.* **2004**, *64*, 1895–1898.
188. Yilmaz, S. Phase transformations in thermally cycled Cu/$ZrW_2O_8$ composites investigated by synchrotron X-ray diffraction. *J. Phys. Condens. Matter* **2002**, *14*, 365–375.
189. Yilmaz, S. Thermal mismatch stress development in Cu-$ZrW_2O_8$ composite investigated by synchrotron X-ray diffraction. *Compos. Sci. Technol.* **2002**, *62*, 1835–1839.
190. Yan, X.; Cheng, X.; Xu, G.; Wang, C.; Sun, S.; Riedel, R. Preparation and thermal properties of zirconium tungstate/copper composites. *Mater. Werkst.* **2008**, *39*, 649–653.
191. Wang, X.; Zhang, J.F.; Zhang, Y.H.; Zhang, J.L.; Lu, F.S.; Wang, X.L. Synthesis and thermal expansion of 4J36/$ZrW_2O_8$ composites. *Rare Met.* **2010**, *29*, 371–375.
192. Kanamori, K.; Kineri, T.; Fukuda, R.; Kawano, T.; Nishio, K. Low-temperature sintering of $ZrW_2O_8$-$SiO_2$ by spark plasma sintering. *J. Mater. Sci.* **2009**, *44*, 855–860.
193. Kofteros, M.; Rodriguez, S.; Tandon, V.; Murr, L.E. A preliminary study of thermal expansion compensation in cement by $ZrW_2O_8$ additions. *Scr. Mater.* **2001**, *45*, 369–374.
194. Yang, X.; Cheng, X.; Yan, X.; Yang, J.; Fu, T.; Qiu, J. Synthesis of $ZrO_2$/$ZrW_2O_8$ composites with low thermal expansion. *Compos. Sci. Technol.* **2007**, *67*, 1167–1171.
195. Yang, X.; Xu, J.; Li, H.; Cheng, X.; Yan, X. In situ synthesis of $ZrO_2$/$ZrW_2O_8$ composites with near-zero thermal expansion. *J. Am. Ceram. Soc.* **2007**, *90*, 1953–1955.
196. Zhang, Z.P.; Liu, H.F.; Cheng, X.N. Study on the technology of $ZrO_2$-$ZrW_2O_8$ composites prepared by co-precipitation method. *J. Inorg. Mater.* **2008**, *23*, 991–995.
197. Yang, X.; Cheng, X.; Li, H.; Xu, J.; Sun, X. Thermal and electric conductivity of near-zero thermal expansion $ZrW_2O_8$/$ZrO_2$ composites. *J. Ceram. Soc. Jpn.* **2008**, *116*, 471–474.
198. Sun, L.; Kwon, P. $ZrW_2O_8$/$ZrO_2$ composites by in situ synthesis of $ZrO_2$ + $WO_3$: Processing, coefficient of thermal expansion, and theoretical model prediction. *Mater. Sci. Eng. A* **2009**, *527*, 93–97.
199. Sun, L.; Kwon, P. $ZrW_2O_8$-$ZrO_2$ continuous functionally graded materials fabricated by in situ reaction of $ZrO_2$ and $WO_3$. *J. Am. Ceram. Soc.* **2010**, *93*, 703–708.

200. Sun, L.; Sneller, A.; Kwon, P. $ZrW_2O_8$-containing composites with near-zero coefficient of thermal expansion fabricated by various methods: Comparison and optimization. *Compos. Sci. Technol.* **2008**, *68*, 3425–3430.
201. Tani, J.-I.; Takahashi, M.; Kido, H. Fabrication and thermal expansion properties of $ZrW_2O_8/Zr_2WP_2O_{12}$ composites. *J. Eur. Ceram. Soc.* **2010**, *30*, 1483–1488.
202. Isobe, T.; Kato, Y.; Mizutani, M.; Ota, T.; Daimon, K. Pressureless sintering of negative thermal expansion $ZrW_2O_8/Zr_2WP_2O_{12}$ composites. *Mater. Lett.* **2008**, *62*, 3913–3915.
203. Isobe, T.; Umezome, T.; Kameshima, Y.; Nakajima, A.; Okada, K. Preparation and properties of negative thermal expansion $Zr_2WP_2O_{12}$ ceramics. *Mater. Res. Bull.* **2009**, *44*, 2045–2049.
204. Tani, J.-I.; Kimura, H.; Hirota, K.; Kido, H. Thermal expansion and mechanical properties of phenolic resin/$ZrW_2O_8$ composites. *J. Appl. Polym. Sci.* **2007**, *106*, 3343–3347.
205. Chu, X.; Huang, R.; Yang, H.; Wu, Z.; Lu, J.; Zhou, Y.; Li, L. The cryogenic thermal expansion and mechanical properties of plasma modified ZrW(2)O(8) reinforced epoxy. *Mater. Sci. Eng. A* **2011**, *528*, 3367–3374.